2 Miy

NASA TECHNICAL NOTE

NASA TN D-7427

NASA TN D-7427

HYPERSONIC AERODYNAMIC CHARACTERISTICS OF A FAMILY OF POWER-LAW, WING-BODY CONFIGURATIONS

by James C. Townsend

Langley Research Center
Hampton, Va. 23665

NATIONAL AERONAUTICS AND SPACE ADMINISTRATION • WASHINGTON, D. C. • DECEMBER 1973

1. Report No.	2. Government Accession No.	3. Recipient's Catalog No.
NASA TN D-7427		
4. Title and Subtitle HYPERSONIC AERODYNAMIC CHARACTERISTICS OF A FAMILY OF POWER-LAW, WING-BODY CONFIGURATIONS		5. Report Date December 1973 6. Performing Organization Code
7. Author(s) James C. Townsend		8. Performing Organization Report No. L-7176
9. Performing Organization Name and Address NASA Langley Research Center Hampton, Va. 23665		10. Work Unit No. 760-66-01-01 11. Contract or Grant No.
12. Sponsoring Agency Name and Address National Aeronautics and Space Administration Washington, D.C. 20546		13. Type of Report and Period Covered Technical Note 14. Sponsoring Agency Code
15. Supplementary Notes		

16. Abstract

The configurations analyzed are half-axisymmetric, power-law bodies surmounted by thin, flat wings. The wing planform matches the body shock-wave shape. Analytic solutions of the hypersonic small disturbance equations form a basis for calculating the longitudinal aerodynamic characteristics. Boundary-layer displacement effects on the body and the wing upper surface are approximated. Skin friction is estimated by using compressible, laminar boundary-layer solutions. Good agreement was obtained with available experimental data for which the basic theoretical assumptions were satisfied. The method is used to estimate the effects of power-law, fineness ratio, and Mach number variations at full-scale conditions. The computer program is included.

17. Key Words (Suggested by Author(s))	18. Distribution Statement
Power-law body Hypersonic flow Wing-body combinations Hypersonic similarity	Unclassified – Unlimited

19. Security Classif. (of this report)	20. Security Classif. (of this page)	21. No. of Pages	22. Price*
Unclassified	Unclassified	47	Domestic, $3.00 Foreign, $5.50

*For sale by the National Technical Information Service, Springfield, Virginia 22151

HYPERSONIC AERODYNAMIC CHARACTERISTICS OF A FAMILY OF POWER-LAW, WING-BODY CONFIGURATIONS

By James C. Townsend
Langley Research Center

SUMMARY

The configurations analyzed are half-axisymmetric, power-law bodies surmounted by thin, flat wings. The wing planform matches the body shock wave shape. Analytic solutions of the hypersonic small disturbance equations form a basis for calculating the longitudinal aerodynamic characteristics. Approximate boundary-layer displacement effects on the body and wing upper surface are included. Skin friction is estimated by using compressible, laminar boundary-layer solutions. By using an effective body shape, the method is extended to small angles of attack. Three basic theoretical assumptions are made: (1) the body is slender, (2) the shock wave is strong, and (3) the Mach number is large. In comparisons with available experimental data, good agreement was obtained when these assumptions were satisfied. The method is also used to estimate the effects of power law, fineness ratio, and Mach number variations at full-scale conditions. The implementing computer program is included.

INTRODUCTION

Much research has been devoted to the hypersonic flow about half bodies of revolution mounted beneath a thin wing. Theoretical studies (refs. 1 to 3) and experimental work (refs. 4 to 7) show that with half-cone bodies these configurations combine good stability characteristics with high values of maximum lift-drag ratio. Replacing the conical bodies with those having power-law profiles generates a larger class of configurations and one which is more representative of aircraft shapes. Low wave-drag bodies in the hypersonic regime are generated by power-law curves with exponent in the range 0.5 to 0.8. (See refs. 8 to 12.) These bodies have the additional advantage of better volume distribution than cones.

The purpose of this study was to develop a method for calculating the longitudinal aerodynamic characteristics of power-law bodies with reflection-plane wings. The method applies to configurations consisting of half of an axisymmetric power-law body mounted beneath a thin wing whose planform matches the theoretical body shock shape at zero angle of attack. Small-disturbance theory, with small perturbations for Mach number and boundary-layer displacement effects, provides a means for calculating the pressure field and shock-wave shape. This pressure field is integrated analytically to obtain the forces and moment on the body. Small angles of attack are simulated, and laminar skin friction is calculated. The computer programs which have been written to implement this method are presented in an appendix.

SYMBOLS

a_1 shock-wave perturbation constant

C Chapman-Rubesin constant, $\dfrac{\mu_w/\mu_\infty}{T_w/T_\infty}$

C_A axial-force coefficient, $\dfrac{\text{Axial force}}{\bar{q}_\infty S}$

C_D drag coefficient, $\dfrac{D}{\bar{q}_\infty S}$

C_L lift coefficient, $\dfrac{L}{\bar{q}_\infty S}$

C_m pitching-moment coefficient, $\dfrac{\text{Pitching moment}}{\bar{q}_\infty S\bar{c}}$

C_N normal-force coefficient, $\dfrac{\text{Normal force}}{\bar{q}_\infty S}$

$C_{N,b}$ normal-force coefficient of body

$C_{N,w}$ normal-force coefficient of wing

C_p pressure coefficient, $\dfrac{\bar{p} - \bar{p}_\infty}{\bar{q}_\infty}$

$\bar{c}$ mean aerodynamic chord, taken as $\bar{c}_b = \dfrac{2\bar{l}}{m + 2}$

D drag

E constant in boundary-layer displacement thickness

F	similarity static-pressure variable
f	fineness parameter, $\frac{\bar{l}}{\bar{r}_{b,B}}$
I	boundary-layer profile parameter
J	integral of F from body to shock
L	lift
$\bar{l}$	length
M_∞	free-stream Mach number
m	exponent of power-law body shape
p	dimensionless static pressure, $\frac{\bar{p}}{2\delta^2\bar{q}_\infty}$
$\bar{\bar{p}}_u$	average wing upper surface pressure
$\bar{q}_\infty$	free-stream dynamic pressure
R	dimensionless shock-wave radius, $\frac{\bar{R}}{\delta\bar{l}}$
$R_{\infty,l}$	free-stream Reynolds number, $\frac{\bar{\rho}_\infty\bar{l}\,\overline{U}_\infty}{\bar{\mu}_\infty}$
r	dimensionless radial coordinate, $\frac{\bar{r}}{\delta\bar{l}}$
S	projected planform area
s_c	distance from nose to upper surface center of pressure
T	temperature
$\overline{U}_\infty$	free-stream axial velocity

V	volume of body
x	dimensionless axial coordinate, $\frac{\bar{x}}{\bar{l}}$
α	angle of attack relative to body axis
γ	ratio of specific heats
δ	shock-wave slope parameter, $\delta \equiv \frac{\bar{R}_{0,B}}{\bar{l}} = \frac{1}{f\eta_b}$
δ^*	dimensionless boundary-layer displacement thickness, $\frac{\bar{\delta}^*}{\delta\bar{l}}$
ϵ_1	small perturbation parameter for Mach number, $\frac{1}{(\delta M_\infty)^2}$
ϵ^*	small perturbation parameter for boundary-layer displacement, $\frac{d\delta^*/d\xi}{dr_b/d\xi}$
η	similarity form of radial coordinate, $\frac{r}{R_0}$
θ	shock-wave angle
$\kappa = \left(\frac{\delta}{\delta_e}\right)^2$	
μ	viscosity coefficient
$\nu = \frac{f_e}{f}$	
ξ	similarity form of axial coordinate
ρ	dimensionless density, $\frac{\bar{\rho}}{\bar{\rho}_\infty}$

Subscripts:

B	at base of configuration, $x = 1$
b	body

e	effective body shape
max	maximum
$(L/D)_{max}$	maximum lift-drag ratio
0	zero-order similarity solution $\left(\epsilon_1 \rightarrow 0\right)$
1	first-order similarity solution $\left(\epsilon_1{}^2 << 1\right)$
∞	free-stream value
w	wall

An asterisk denotes that the quantity includes boundary-layer displacement effect. A bar over a symbol denotes a dimensional quantity.

THEORY

The method applies to the general configuration shown in figure 1(a). It consists of one-half of a body of revolution mounted beneath a thin wing at an angle of attack of 0°. By assumption, the wing acts as an endplate to maintain the axial symmetry of the flow about the body. The wing planform matches the shock-wave shape about the full body, and the body pressure field acts on the wing to provide additional lift. The method is put together from a series of pieces in order to arrive at the final aerodynamic coefficients. The basis for the development is the result in hypersonic slender-body theory that for power-law bodies, there are similarity solutions to the inviscid flow equations in the hypersonic limit. (See ref. 13.) Independent small perturbations are made to account for Mach number effects and for laminar boundary-layer displacements. (See ref. 14.) To simulate the effects of small angles of attack, a simple substitution of an effective body is made. The resulting equation for the pressure distribution is integrated analytically to obtain the pressure forces and moments on the body. Then the laminar skin-friction drag is calculated by using the analytic pressure distribution. The development outlined is explained in more detail in the following sections.

Inviscid, Power-Law Body Solution

If, in inviscid hypersonic flow about a slender body, the velocity changes in the free-stream direction are neglected compared with the transverse flow velocities, the hypersonic small-disturbance equations result. When a strong, power-law shock wave occurs in such a flow at infinite Mach number, these equations indicate that the body generating the shock also has a power-law shape. (See ref. 14.) Thus in figure 1(a), the shock wave $\frac{\bar{R}_0}{l} = \delta\left(\frac{\bar{x}}{l}\right)^m$ is generated by the body $\frac{\bar{r}_b}{l} = \frac{1}{f}\left(\frac{\bar{x}}{l}\right)^m$. In dimensionless form (fig. 1(b)) these relations become $R_0 = x^m$ and $r_b = \frac{1}{\delta f} x^m$. When the dependent variables are expressed in terms of the slope of the shock wave, the axial variations may be separated from the radial variations of the variables to obtain similarity equations. Thus in similarity variables $\xi = x$ and $\eta = r/R_0$; $R_0 = \xi^m$, $r_b = \eta_b \xi^m$, and the dimensionless pressure field is $p_0 = F_0(\eta)\left(\frac{dR_0}{d\xi}\right)^2 = m^2 F_0(\eta)\, \xi^{2(m-1)}$. Here $F_0(\eta)$ is found by solving a set of ordinary differential equations in η. (See refs. 14 and 15.)

In order to relax the restriction to infinite Mach number, Kubota (ref. 14) applied a small perturbation procedure. This procedure results in the following first-order pressure distribution and shock-wave shape about the power-law body $r_b = \eta_b x^m$:

$$p_1(\xi,\eta) = m^2 F_0(\eta)\ \xi^{2(m-1)} + \epsilon_1 m^2 F_1(\eta) \tag{1}$$

$$R_1(\xi) = \xi^m \left[1 + \epsilon_1 a_1 \xi^{2(1-m)}\right] \tag{2}$$

Here $\epsilon_1 \equiv (M_\infty \delta)^{-2}$ is a small parameter corresponding to the hypersonic strong shock assumption $M_\infty \sin\theta >> 1$. The necessity of simultaneously satisfying $\delta^2 << 1$ and $\epsilon_1{}^2 << 1$ puts a strong requirement on the Mach number. That is, the present method is limited to $M_\infty >> 1$ so that with a slender body $\delta^2 << 1$, the parameter ϵ_1 is still small. Figure 2 shows the relationship between δ, ϵ_1, and M_∞ and can be used to check on ϵ_1 for a given Mach number and body shape (by noting that $\delta = 1/f\eta_b$).

The perturbed pressure variable $F_1(\eta)$ and the shock-wave displacement constant a_1 are found from a second set of ordinary differential equations. (See refs. 14 and 15.) The two sets of differential equations involve only m and γ as parameters, and thus they can be solved over the needed range of values and the tabulated results used in applications to flow problems. Table I and figure 3 present the results needed for the current application. They were found by numerical integration techniques similar to those described in reference 16. (With acess to modern digital computers, the exact numerical computation has become at least as easy to carry out as the approximate technique which gives ref. 16 its title.) The integrated pressure J_0 and pressure perturbation J_1 are defined as $J_0 \equiv \int_{\eta_b}^1 F_0(\eta)\, d\eta$ and $J_1 \equiv \int_{\eta_b}^1 F_1(\eta)\, d\eta$; they will be applied to the wing undersurface.

Corrections for Boundary-Layer Displacement

In order to make a corrected approximation accounting for laminar boundary-layer growth, a perturbed body shape $r_b^*(x) = r_b + \delta^*$ is used. The displacement thickness of the boundary layer is given by $\delta^* = \frac{2m\eta_b}{3 - 2m} Ex^{3/2-m}$ (based on a result from ref. 17 for adiabatic wall conditions). Here $E \equiv \frac{\gamma - 1}{\sqrt{2\gamma}} M_\infty f^2 I\eta_b \frac{3 - 2m}{2m^2\sqrt{4m - 1}}\sqrt{\frac{C}{R_{\infty,l} F_0(\eta_b)}}$ which is very small for large Reynolds numbers. By using the appropriate value for I (the sum of the transformed displacement and momentum thicknesses in refs. 18 and 19), this relation for δ^* may be applied for any constant wall temperature. If the flow outside the boundary layer is considered to be the inviscid flow about the "perturbed body" $r_b^*(x)$, the corresponding pressure distribution and shock shape are approximated as follows. In terms of the body radius $r_b = \eta_b\xi^m$, equations (1) and (2) become

$$p_1 = m^2F_0(\eta)\xi^{2(m-1)} + \epsilon_1 m^2F_1(\eta) = \frac{F_0(\eta)}{\eta_b^2}\left(\frac{dr_b}{d\xi}\right)^2 + \epsilon_1 m^2 F_1(\eta)$$

and

$$R_1 = \xi^m\left[1 + a_1\epsilon_1\xi^{2(1-m)}\right] = \frac{r_b}{\eta_b}\left[1 + a_1\epsilon_1\left(\frac{1}{m\eta_b}\frac{dr_b}{d\xi}\right)^{-2}\right]$$

By replacing r_b by r_b^* (as in ref. 14), these equations become

$$p_1^*(\xi,\eta) = \frac{F_0(\eta)}{\eta_b^2}\left(\frac{dr_b^*}{d\xi}\right)^2 + \epsilon_1 m^2F_1(\eta) = m^2\xi^{2(m-1)}(1 + \epsilon^*)^2F_0(\eta) + \epsilon_1 m^2F_1(\eta) \tag{3}$$

and

$$R_1^*(\xi) = \frac{r_b^*}{\eta_b}\left[1 + a_1\epsilon_1\left(\frac{1}{m\eta_b}\frac{dr_b^*}{d\xi}\right)^{-2}\right]$$

$$= \xi^m\left[1 + \frac{\delta^*}{r_b} + a_1\epsilon_1\xi^{2(1-m)}\right] + \text{terms of order } \epsilon_1\epsilon^* \tag{4}$$

Here $\epsilon^* \equiv \frac{d\delta^*/d\xi}{dr_b/d\xi} = E\xi^{\frac{3}{2}-2m} << 1$ except in a small region near the nose when $m > \frac{3}{4}$.

Simulation of Angle of Attack

The pressure distribution along the pitch plane of the body at angle of attack is assumed to be the same as that about an equivalent axisymmetric body. This effective body is at zero angle of attack. It has a power-law profile which closely matches the windward element in the plane of symmetry of the actual body at angle of attack. Figure 4 shows the relation between the real and effective bodies, and the following expressions are used to obtain the effective body parameters

$$\left.\begin{aligned}
\bar{x}_e &= \bar{x}\cos\alpha - \bar{r}_b \sin\alpha \\
\bar{r}_{b,e} &= \bar{x}\sin\alpha + \bar{r}_b\cos\alpha \\
f_e &\equiv \frac{\bar{l}_e}{\bar{r}_{b,e,B}} = \frac{1 - \frac{1}{f}\tan\alpha}{\tan\alpha + \frac{1}{f}} \approx \frac{f}{1 + f\tan\alpha} \qquad (\tan\alpha \ll 1)
\end{aligned}\right\} \tag{5}$$

and

$$m_e \equiv \frac{\log_e\left(\bar{r}_{b,2,e}/\bar{r}_{b,1,e}\right)}{\log_e\left(\bar{x}_{2,e}/\bar{x}_{1,e}\right)}$$

so that

$$\frac{\bar{r}_{b,e}}{\bar{l}_e} \approx \frac{1}{f_e}\left(\frac{\bar{x}_e}{\bar{l}_e}\right)^{m_e}$$

Here $\bar{x}_1$ and $\bar{x}_2$ are points selected to provide a good approximation. A lower limit of $m_e \geqq 0.51$ was set to avoid computational problems associated with the theoretical limit as $m \to 0.5$.

The approximating pressure distribution along the body at angle of attack is then

$$p^*_{1,e}\left(\eta_{b,e}\right) = \frac{{m_e}^2}{\kappa}\left[\left(1 + 2\nu^2 E_e {x_e}^{\frac{3}{2} - 2m_e}\right) F_0\left(\eta_{b,e}\right) {x_e}^{2\left(m_e - 1\right)} + \kappa\epsilon_1 F_1\left(\eta_{b,e}\right)\right] \tag{6}$$

where

$$\nu \equiv \frac{f_e}{f} = \frac{1}{1 + f\tan\alpha}$$

$$\kappa \equiv \left(\frac{\delta}{\delta_e}\right)^2 = \nu^2\left(\frac{\eta_{b,e}}{\eta_b}\right)^2$$

and E_e is the same as E with m_e replacing m. $\left(\text{The factor } \kappa \text{ appears since } p_{1,e}^{*} \equiv \frac{\overline{p_{1,e}^{*}}}{2\bar{q}\delta^2} = \frac{1}{\kappa} \frac{\overline{p_{1,e}^{*}}}{2\bar{q}\delta_e^{2}}.\right)$ By following reference 6 which uses a similar angle-of-attack method for half-cone wing configurations, this pressure distribution is applied over the entire body surface. The pressure distribution under the wing from $\eta_b \leqq \eta \leqq 1$ is assumed to be the same as that in the flow field of the effective body from $\eta_{b,e} \leqq \eta \leqq 1$. Since this equivalent body approach does not attempt to account for the actual flow under the wing, its use necessarily limits the present method to very small angles of attack. For this reason all calculated results presented are in the range $\frac{1}{2} \leqq \nu \leqq 2$. Instead of calculating the wing upper surface pressure in detail, an average pressure is used. This value is taken from the charts of reference 20, which includes viscous-interaction effects on the pressure and skin friction on delta wings at angle of attack in hypersonic flow. Since the viscous effects are approximately proportional to $x^{-1/2}$, delta-wing results for which $\iint x^{-1/2}\,dr\,dx$ and the span equal to those of the power-law wing are used. The base pressure is set equal to free-stream static pressure p_∞.

Skin Friction

The skin-friction contribution is the remaining term of the axial-force coefficient to be evaluated. In this report laminar boundary layers are assumed for all calculations. The wetted area is divided into the body surface, wing upper surface, and the exposed part of the wing underside, each of which is treated separately. For the skin-friction calculations for the body and the wing lower surface, the longitudinal pressure distribution is modified in the nose region by keeping a higher order term in the pressure equation. These calculations then use a scheme given in reference 18 for incompressible laminar boundary layers. Two transformations of the independent variables allow its use with the two-dimensional compressible laminar-boundary-layer similar solutions of reference 19 for the present cases. For the body, the Mangler transformation (ref. 18) changes the axial coordinate to that for an equivalent two-dimensional body. For the relatively small exposed-wing undersurface, a simplified flow model is applied, that is, streamlines are taken as parallel to the body surface, and the pressure is taken as varying parabolically from the body to the shock wave. In both cases the Stewartson transformation (ref. 19) changes the surface length and exterior velocity distribution to the form for an equivalent incompressible flow; the method of reference 18 is then applied. For the wing upper surface, the average skin friction from the appropriate charts of reference 20 is used just as for the upper surface pressure.

Longitudinal Aerodynamic Coefficients

Integrations of the appropriate components of the surface pressures over the body and wing give expressions for the axial force, the normal force on the body and on the wing, and the pitching moment. In coefficient form the expressions are (to first order in ϵ_1 and ϵ^*):

$$C_A = \frac{\pi(m+1)\delta^2 m_e^2}{f\kappa \frac{S}{S_b}}\left\{\left[\frac{1}{2(m_e+m-1)} + \frac{4\nu^2 E_e}{4m-1}\right] mF_0(\eta_{b,e}) + \frac{\epsilon_1\kappa}{2}\left[F_1(\eta_{b,e}) - \frac{1}{\gamma m_e^2}\right]\right\} + C_{A,F}$$

$$C_{N,b} = \frac{2m_e^2\delta^2}{\kappa \frac{S}{S_b}}\left\{\left(\frac{1}{2m_e+m-1} + \frac{4\nu^2 E_e}{2m+1}\right)(m+1)F_0(\eta_{b,e}) + \epsilon_1\kappa\left[F_1(\eta_{b,e}) - \frac{1}{\gamma m_e^2}\right]\right\}$$

$$C_{N,w} = \frac{2m_e^2\delta^2}{\kappa \frac{S}{S_b}}\left(\left\{\left(\frac{1}{2m_e+m-1} + \frac{4\nu^2 E_e}{2m+1}\right)\left(\frac{1-\eta_b}{1-\eta_{b,e}}\right)J_{0,e} + \frac{2}{\gamma+1}\left[\frac{4mE}{(3-2m)(4m_e-2m+1)}\right.\right.\right.$$

$$\left.\left.\left. + \frac{\epsilon_1 a_1}{2m_e-m+1}\right]\right\}(m+1) + \epsilon_1\kappa\left(\frac{1-\eta_b}{1-\eta_{b,e}}J_{1,e} - \frac{1-\eta_b}{\gamma m_e^2}\right)\right)$$

$$C_N = C_{N,b} + C_{N,w} - \frac{\bar{\bar{p}}_u - p_\infty}{q_\infty}$$

$$C_m = -\frac{(m+1)(m+2)m_e^2\delta^2}{\kappa \frac{S\bar{c}}{S_b\bar{c}_b}}\left\{\frac{1}{f^2}\left(\frac{1}{2m_e+3m-2} + \frac{4\nu^2 E_e}{6m-1}\right)mF_0(\eta_{b,e})\right.$$

$$+ \frac{\epsilon_1\kappa}{3f^2}\left[F_1(\eta_{b,e}) - \frac{1}{\gamma m_e^2}\right] + \left(\frac{1}{2m_e+m} + \frac{4\nu^2 E_e}{2m+3}\right)\left[F_0(\eta_{b,e}) + \frac{1-\eta_b}{1-\eta_{b,e}}\frac{\bar{J}_{0,e}}{\eta_b}\right]$$

$$+ \frac{2}{(\gamma+1)\eta_b}\left[\frac{4mE}{(3-2m)(4m_e-2m+3)} + \frac{\epsilon_1 a_1}{2m_e-m+2}\right] + \frac{\epsilon_1\kappa}{m+2}\left[F_1(\eta_{b,e})\right.$$

$$\left.\left. + \frac{1-\eta_b}{1-\eta_{b,e}}\frac{J_{1,e}}{\eta_b} - \frac{1}{\gamma m_e^2 \eta_b}\right]\right\} + \frac{\bar{\bar{p}}_u - p_\infty}{q_\infty}\frac{s_c}{\bar{c}}$$

The pitching-moment reference center is at the nose of the body ($x = 0$). For the corresponding zero-order and inviscid relations, set $\epsilon_1 = 0$ and $E = 0$, respectively. Note that the factors η_b and $m + 1$ are associated with the actual planform area used in normalizing the coefficients.

These equations have been programed for calculation by a high-speed digital computer. The program includes the skin-friction calculations on the body and the wing undersurface. There is a subsidiary program which computes the parameters required to get the upper surface pressure and skin friction from reference 20. The appendix presents an exposition of these programs. The basic program requires only 21 600 octal storage locations after compilation on the Control Data Corporation 6600 computer at the Langley Research Center and runs an average case with 11 angles of attack in about 3 seconds of central processor time.

DISCUSSION OF RESULTS

Evaluation of Method

There have been no reported comprehensive experimental evaluations of the power-law, wing-body configurations to which the theoretical analysis applies. The data available fall into two groups: (1) drag of complete power-law bodies of revolution (no wing) at several Mach numbers and fineness ratios, and (2) aerodynamic characteristics of conical ($m = 1.0$) wing-body configurations. Only a small part of these data satisfy the high Mach number, the slender body, and the strong shock criteria required for strict application of the similarity theory. Data for which the criteria are not well satisfied can be used to determine the limits for practical application of the method.

Power-law bodies of revolution.- The zero-angle-of-attack drag of these bodies is already calculated as part of the present method. Figure 5 contains four sets of comparisons with experimental data. The drag coefficients have been based on the length squared as reference area in each case to form a uniform basis of comparison. In parts (a) and (b) of figure 5, the ratio V/l^3 was held constant and yielded a small variation in the fineness ratio as the power-law exponent was varied to obtain the different bodies for the tests. Figure 5(a) is for tests at Mach 21.6 in helium (ref. 12). The agreement is very good. The coefficients in figure 5(b) are for tests at Mach 10.03 in air (ref. 21); the calculations are in good agreement with experiment. Figure 5(c) shows good agreement at Mach 10.35 for a series of power-law bodies having nearly equal fineness ratios. In figure 5(d) the data for the same bodies at Mach 5.96 is not predicted.

The range of agreement obtained in figure 5 should be considered in light of the basic assumptions of the theory as discussed in the previous section. For this reason the pertinent parameters are shown in the legends of figure 5 and also in figure 2. Since $\delta << 1$ for all cases, the slender body condition is well satisfied. The hypersonic assumption $\left(M_\infty >> 1\right)$ is generally considered to be satisfied for $M > 5$ and so should not cause the discrepancies in figure 5. However, the strong shock assumption $\left(\epsilon_1^{\,2} << 1\right)$ is satisfied only for figure 5(a), where the agreement is very good. This result shows the importance of evaluating ϵ_1 to determine whether the theory can reasonably be applied to any particular configuration and free-stream conditions.

As an additional comparison with the present method and the experimental data, drag coefficients based on the simple Newtonian pressure equation $C_p = 2 \sin^2\theta_b$ and on inviscid conical flow were calculated and are presented in figure 5. The Newtonian prediction and inviscid conical solution drag values are low since viscous interaction effects on the surface pressure become important on high-fineness-ratio bodies at high Mach numbers.

As noted in reference 22, entropy layer effects become important for power-law exponents less than $m = \frac{\gamma + 1}{2\gamma + 1}$ ($m \approx 0.63$ for $\gamma = 1.4$); therefore, the theoretical predictions (which do not include these effects) can be expected to be poorer in that range. A less subtle limitation occurs at $m = 0.5$, where $\eta_b = 0$; that is, the ratio of shock-wave radius to body radius becomes infinite. This case is the "blast wave" solution for blunt-nosed bodies of negligible thickness (for example, a cylindrical rod) as described in references 15 and 22. For bodies with nonzero radius, as in figure 5, the predicted shock-wave radius goes to infinity as $m \rightarrow 0.5$ and so does the wave drag. Thus, the theory is not useful for the blunter shapes.

Wing, conical-body configurations.- Theoretical estimates for wing conical body configurations can be compared with the experimental data in reference 23. The bodies in this reference were halves of right, circular cones, corresponding to $m = 1$. The wings were thin flat plates. The normal- and axial-force coefficients for configurations with the first-order Mach number and boundary-layer thickness corrections to the wing planform shapes are presented in figure 6. The present theory is in good agreement with the experimental data near an angle of attack of 0°, but deviates from it elsewhere. The deficiency in the angle-of-attack method is such that the errors in C_A and C_N are generally about equal and in the same direction. This condition results in the good prediction of the lift-drag curve (drag polar) shown in figure 7, which produces lift-drag ratios agreeing well with the experimental values. Figure 7 also shows the pitching-moment coefficient, the theory generally agreeing well with experiment near $\alpha = 0^{\circ}$.

Other data for comparison with theory may be found in references 6 and 7. The wings for the configurations tested had delta planforms with several leading-edge sweeps. Consequently, they cannot match the shapes used by the theory, but at small angles of attack, where the wing alone produces little lift or drag, the aerodynamic coefficients should be comparable if they are based on the areas of delta wings approximating the theoretical planforms. Figure 8 shows such a comparison at Mach numbers 6.86 (ref. 6) and 20 (ref. 7). The theoretical drag polars and the lift variation with angle of attack at $M = 6.86$ agree well with the experimental points, especially near $\alpha = 0^{\circ}$ (fig. 8(a)). The pitching moment about $x = 2l/3$ is predicted well near $C_L = 0$, but the slope shows an almost neutrally stable trend whereas the experimental data show the configuration to be somewhat more stable. The difference in the distribution of wing area between the experiment and theory would contribute to this effect.

Maximum lift-drag ratios for the same configurations (and some with smaller cone angles) in helium at Mach 20 are shown in figure 8(b). The predicted values agree fairly well with experiment considering the differences in wing shape and area.

Example Application of Method

The preceding comparisons with experimental results have shown that the present theoretical method gives good predictions of the lift, drag, and lift-drag ratio and fair estimates of the pitching moment for small angles of attack as long as the basic assumptions of the theory are met. Thus, the method should be useful for studying the general characteristics of the power-law-body flat-wing configurations at high Mach numbers. Just two parameters, the power-law exponent m and the fineness parameter f, completely specify these body shapes. For the wings the Mach number is the principal additional parameter required, although the Reynolds number, ratio of specific heats, and wall temperature also enter through the boundary-layer growth perturbation. In order to assess the effects of these three main variables, the theory was used to predict the aerodynamic characteristics of a family of full-scale configurations at two Mach numbers. The chosen altitude was 30 km for which the unit Reynolds numbers are 2.21×10^6/meter and 4.42×10^6/meter at the chosen Mach numbers of 6 and 12, respectively, based on the 1962 standard atmosphere (ref. 24). The body volume was set at 2500 m^3, giving lengths of 28.2 m to 78.1 m (approximately 92.5 ft to 256 ft), for $0.63 \leqq m \leqq 1$ and $2.5 \leqq f \leqq 10.0$. Additional assumptions were $\gamma = 1.4$ and a ratio of wall temperature to total temperature of 0.41667. For each Mach number the range of the fineness parameter was chosen to keep $\delta^2 << 1$ and $\epsilon_1{}^2 << 1$. The results of these calculations are presented in figures 9 and 10.

Effect of power-law exponent.- Varying the body power-law exponent while holding the fineness parameter constant at $f = 5$ for Mach 12 flight at an altitude of 30 km produced the curves shown as figure 9(a). The drag polars in the range $0.63 \leqq m \leqq 0.75$ all cluster together, and hence so do the lift-drag ratios. Only in the conical case ($m = 1$) does the drag fall significantly higher and the lift-drag ratio lower. The pitching moment does show a major variation with m, both in slope and intercept. As m decreases from 1.0 to 0.63, that is, as the nose becomes blunter and the aft end less flared, the zero lift pitching moment $C_{m,0}$ increases. At the same time, the stability decreases, configurations with $m < 0.75$ becoming unstable for the moment reference center at $\bar{x} = 0.6\bar{l}, \bar{y} = 0.15\bar{r}_{b,B}$. Since the effect of m on the lift-drag ratio is relatively small, this parameter could be chosen to minimize the trim drag.

Effect of fineness ratio.- The computed characteristics for a range of values of the fineness parameter f are shown in figure 9(b). For this family of configurations, the power-law exponent was set at $m = 0.75$, and the curves are for Mach 12 flight at 30 km as before. At low values of f the peaks in L/D are low and broad and become higher and sharper as the bodies become finer. The stability of the configurations is practically unaffected by variations in the fineness parameter, as indicated by the almost parallel pitching-moment curves.

Effect of Mach number.- Figure 9(c) shows a comparison of Mach 6 calculations with those for Mach 12 for configurations having three of the power-law body shapes. Note that the change in Mach number makes a change in the wing planform for each body shape. The effect on the drag polars shows clearly in the three sets of curves. At Mach 6 the zero lift-drag coefficient $C_{D,0}$ is higher but the drag due to lift is lower than at Mach 12. Since the curves cross before $(L/D)_{max}$ is reached, the Mach 6 curves of L/D peak higher and at larger C_L values than the Mach 12 curves. If the same reference area had been used, the C_L difference would have been larger since the Mach 12 design wing is smaller. The pitching-moment curves are little affected by the Mach number change.

Summary of calculations.- The results of the Mach 6 and 12 calculations for flight at 30 km are summarized in figure 10. As was indicated in figure 9, the effect of the power-law exponent m on $(L/D)_{max}$ is relatively small. For the low fineness ratios, the curves form broad maxima centered near $m = 0.7$; they become more peaked and move toward $m = 0.8$ as the fineness ratio increases. This result compares with the value $m = 0.75$ determined from the Newtonian pressure law as the power-law exponent for minimum drag bodies under length and diameter (that is, fineness ratio) constraints. There is a stronger dependence of the associated lift coefficient $C_{L,(L/D)_{max}}$ on the value of m, particularly for the less fine bodies. The effect of the fineness parameter on $(L/D)_{max}$ and $C_{L,(L/D)_{max}}$ is opposing in that increasing f increases $(L/D)_{max}$ (and its dependence on m) but decreases $C_{L,(L/D)_{max}}$ (and its dependence on m). (At any given lift coefficient in the range of calculation, however, L/D can be increased by going to a finer body; see fig. 9(b).) The curves of $\alpha_{(L/D)_{max}}$ are included in figure 10 in order to show that the calculations of $(L/D)_{max}$ occur within the range of small angles of attack for which the present method gives its best results. (See fig. 6.)

CONCLUDING REMARKS

This paper has presented a method for calculating the longitudinal aerodynamic characteristics of a family of configurations in hypersonic flow. These configurations each consist of a half-axisymmetric power-law body surmounted by a thin flat wing for which the planform matches the analytical shock-wave shape about the body at an angle of attack of 0°. The method is based on the power-law similarity solutions of the hypersonic small-disturbance equations. These solutions require three basic assumptions: the Mach number is large, the body is slender, and the shock wave is strong. A first-order perturbation allows the calculation of Mach number effects, and a perturbation to the body shape provides for the boundary-layer growth. Skin friction is accounted for by using compressible, laminar boundary-layer solutions at the computed pressure distributions integrated over the body and wing surfaces. A computer program has been written implementing this method; sample computations using the program have taken only a few seconds per case.

When compared with experimental data for axisymmetric power-law bodies and for wing—conical-body configurations, the present method gave good agreement where the basic assumptions were satisfied. An example series of computations with variations in the principal parameters at a full-scale flight condition showed that varying the power-law exponent has a greater effect on longitudinal stability and trim than on the lift-drag ratio. The computations for Mach 6 gave higher maximum lift-drag ratios, higher drag coefficients at zero lift, but essentially the same stability characteristics as their counterparts for Mach 12.

Langley Research Center,
National Aeronautics and Space Administration,
Hampton, Va., October 25, 1973.

APPENDIX

COMPUTER PROGRAM FOR CALCULATING THE AERODYNAMIC CHARACTERISTICS OF POWER-LAW WING-BODY CONFIGURATIONS

The calculation procedure described in the main body of the paper for obtaining the aerodynamic coefficients for power-law wing-body configurations at hypersonic speeds has been programed for high-speed digital computation. The program will also compute the zero angle-of-attack drag for an axisymmetric power-law body alone. The purpose of this appendix is to provide a description of the necessary input and available output as well as a FORTRAN IV (ref. 25) listing of the source program. A separate program to compute the parameters needed to obtain two input values from the figures of reference 20 is also listed and described.

Description of Program

First, the program reads all the input variables describing the case to be computed. After calculating geometric constants, it goes through the angles of attack, computing the body axis forces and moments, interpolating the similarity solution parameters from a stored table. Skin friction is calculated for each angle of attack and added to the axial force. The results are then transformed to the stability axes. If at least three angles of attack are included in a case, a quadratic interpolation of the drag polar is made to obtain $(L/D)_{max}$ and other quantities, which are printed out along with the body- and stability-axis coefficients. A summary subroutine assembles certain quantities for separate printout after completion of all cases.

Program Listing

The FORTRAM IV listing of the source program used on the Control Data series 6600 computer system at the Langley Research Center is as follows:

```
      PROGRAM HYPAERO(INPUT=201,OUTPUT=401,TAPE5=INPUT,TAPE7=601)
C
C     HYPERSONIC AERODYNAMIC CHARACTERISTICS OF POWER-LAW WING-BODY CONFIGURATIONS
C
      DIMENSION HEAD(8), Y(6), YE(5), VARD(13,6), VARI(13), ANGL(11),
     1 SINE(11), COSE(11), PBBPOL(11), CFDCF01(11), PUPIOI(11), CNB(11),
     2 CND(11), CNW(11), DPSBYQS(11), CN(11), CAP(11), CAF(11), CA(11),
     3 CL(11), CD(11), CLCD(11), CMCG(11), CDANGL(11,2), CDALO(2),
     4 CDALN(2), X(19), XW(19), PB(19), DSWCOS(19), DSWCSL(7,6),
     5 CCSSL(18), TXSE(18), DELR(18), PTWP1(18)
      EQUIVALENCE (Y,ETAB), (Y(2),FO), (Y(6),A1), (YE,ETABE),
     1 (YE(2),FOE), (YE(3),F1E), (YE(4),DJOE), (YE(5),DJ1E),
     2 (ANGL,CD(12),CDANGL(12))
```

```
      COMMON AP,Z1ME,E2U2,FOE,F1EK,THG12G,TWM,EMBF2,D2ME2K,X2M,WING,F01,
     1 F11K,DLR,ETB,ONETB,XSE,GMA,GM1,GM12,GP12,EM,EMI,EM32,ZMM,ZEMI1,
     2 THP2M,AMCH2,DEL,TWEM,AEP
      NAMELIST /DATA/NCASE,GAM,TINF,AMCH,NALF,ANGL,EM,F,REL,SSB,XCG,YCG,
     1 PBPI,CAFACTR,ANGO,XOUT,PBBPOL,CFDCF01,ALAMCR,BDYONLY,DEL,EPS,XSE
     2 /CUT/T,ANG,ANGO,EME,YE,EMI,CAFB2,CAFU,CAFL,AI,PTWP1
C     VARI = EM, VARD = ASSOCIATED VALUES OF ETAB,F0,F1,DJ0,DJ1,A1 FROM TABLE I
      DATA X/0.,.0003,.0006,.0009,.0012,.0018,.0024,.0036,.005,.0085,
     1 .015,.025,.045,.08,.14,.25,.45,.7,1./, PI,PIF,DTOR/3.14159265359,
     2 2.6586808,.01745329252/, KP,LLIM,ML,ML1,NCASE/-1,19,18,17,1/,
     3 VARI,VARD/1.,.95,.9,.85,.8,.75,.7,.666667,.633333,.6,.55,.53,.51,
     4 .914934,.91034,.90465,.89743,.88798,.87507,.85648,.8388,.81391,
     5 .77647,.66414,.56901,.37221, .87445,.84711,.8163,.78174,.74265,
     6 .69806,.64662,.60763,.56403,.51478,.42678,.385,.33757, .9179,
     7 1.0591,1.2306,1.4386,1.6887,1.9811,2.2986,2.4964,2.6392,2.6593,
     8 2.251,1.8876,1.411, .07323,.07589,.07909,.08303,.08799,.09444,
     9 .10318,.11098,.12129,.13554,.17318,.20119,.25443, .0841,.09551,
     X .11044,.13067,.15918,.20098,.26458,.32562,.40794,.51763,.74598,
     1 .86687,1.0411, .47549,.52709,.58604,.65291,.72741,.80732,.88631,
     2 .93216,.96566,.98034,.96791,.96377,.97539/,              GAM/1.4/,
     3 SSB,TWTT,PBPI,CAFACTR,XE,XOUT/0.,.416667,1.,1.,.10,.FALSE./
      LOGICAL IFMIN,BDYONLY,WING,XOUT
      EXTERNAL FUN1
      BDYONLY=.FALSE.
1     READ 38, HEAD
      IF (ENDFILE 5) 32,2
2     READ DATA
      CLDMX=0.
      COMIN=1.
      IFMIN=.FALSE.
      GO TO (3,4,5,6), NCASE
C     NCASE = 1) GAM,  2) AMCH,TINF,  3) EM,  4) F,REL,SSB  HAVE NEW VALUES
3     GM1=GAM-1.
      ZGM1=2./GM1
      GM12=.5*GM1
      GP1=GAM+1.
      GP12=.5*GP1
      F01=1./GP12
      GMA=GAM
      GP14=.25*GP1
      ZGG1=GAM*ZGM1
      ZG1G=-4./ZGG1
      GMI=1./GAM
      ZG2G=GMI-.5
      GP1G=GP1*GMI
      GF=.12*(2.*GAM)**1.5*GP12**GP1G
      GX1=-GM1*GMI
      G37=-.37/GX1
      THG12G=1.-.5*GX1
      RT8GI=1./SQRT(8.*GAM)
      AT1=1.217*TWTT+.4704
      AT2=TWTT+.346
      RTTWTT=SQRT(TWTT)
4     AMCH2=AMCH*AMCH
      AMCH3=AMCH*AMCH2
      AMI=1./AMCH2
      TTBTI=1.+GM12*AMCH2
      RTTTBTI=SQRT(TTBTI)
      SUTH=198.6/(TINF*TTBTI)
      ALAM=((1.+SUTH)/(TWTT+SUTH))*RTTWTT
      SUTHI=198.6/TINF
      C2=((1.+SUTH)/(1.+SUTHI))*RTTTBTI
      RTC1=SQRT(ALAM/C2)
      TPTI=.273+(.195+.532*TWTT)*TTBTI
      RTC3=SQRT((1.+SUTHI)/(TPTI+SUTHI)*SQRT(TPTI))
      GCMG=GF*RTC1*AMCH**GP1G
      P0=2.*AMI*GMI
```

```
5     EMP1=EM+1.
      EMP12=.5*EMP1
      EMP2=EM+2.
      EMM1=EM-1.
      ZMM1=2.*EMM1
      TWM=2.*EM
      THR2M=3.-TWM
      ZMM=2.-EM
      EMI=1./EM
      ZEMI1=2.*(EMI-1.)
      EM32=1.5*EMI-2.
      ZGM132=1.5+ZMM1*GMI
      ZMP1I=1./(EMP1+EM)
      TWM3I=1./(EMP1+EMP2)
      EM4I=1./(4.*EM-1.)
      SIXMI=1./(6.*EM-1.)
      THRMMI=1./(3.-EM)
      FIV2MI=1./(5.-TWM)
      EM4019=.4019*EM
      EMX1I=1./(1.5303-EM4019)
      EMX152M=FIV2MI/EMX1I
      EMX2=.5/(.9274+EM4019)
      IP=20.*(1.05-EM)
      AI=AI1-AI2*EMM1/(EMM1-G37/EM4I)
      CALL MTLUP (EM,Y,2,13,13,6,IP,VARI,VARD)
      ETABI=1./ETAB
      ONETET=ETABI-1.
      ZG1ET=ETABI/GP12
      ETB=ETAB
      ONETB=1./(1.-ETAB)
      AMCHN=(1.-ZMM1*(AMCH-1.))**GMI
      GETIEMF=GCMG*ETAB*AI*SQRT(EM4I)*(EM*EM*FO)**ZG2G/AMCHN
      F11=FOI*(AI*(ZGG1+2./GP1G-EMI/GM1)-EMI*EMI/ZGG1)
6     FI=1./F
      EMBF2=(EM*FI)**2
      FSQ=F*F
      EM1M2F2=EMP1*EMP2/FSQ
      RTRELI=1./SQRT(REL)
      ESAV=GM1*AMCH*FSQ*RTC1*RTRELI*RT8GI
      DEL=ETABI*FI
      EPS=AMI/(DEL*DEL)
      AEP=AI*EPS
      EMSAV=4.*ESAV*AI*ETAB/(EM*SQRT(FO/EM4I))
      TWEM=EMSAV*.5
      RSE=SQRT(GETIEMF*RTRELI*DEL**ZG1G*XE**ZGM132)
      PT2P1=PTOT(RSE)
      RTROLI=SQRT(AMCH*RTTTBTI**3/(C2*REL*PT2P1))
      AEPX=AEP*EMX152M
      EM32X=.25*EMSAV*EMX1I
      G2MRC=.69053*GM12*AMCH3*RTC3*RTRELI
      EMFSAV=0.
C
C   WING GEOMETRIC PARAMETERS AND FLOW CONSTANTS
C
      S1STSB=ETABI*(1.+EMP1*(AEP*THRMMI+EMSAV*FIV2MI))
      SBBYS=1./S1STSB
      IF (SSB.GT.0.) SBBYS=1./SSB
      S1STBYS=S1STSB*SBBYS
      DEL2=DEL*DEL
      PIMS=.5*PI*EMP1*SBBYS
      RTCRELI=SQRT((1.+AEP+TWEM)/(PIF*(EMX2+AEPX+EM32X)))
      XSC=EMP12
      ALAMCR=G2MRC*RTCRELI
      POLAM=-PO*ALAMCR
      CFOCR=1.328*RTC1*RTRELI*RTCRELI*S1STBYS
      CAFLC=2.*ALAM*AMI*RTROLI
      CFCON=PT2P1*CAFLC
```

```
      EMETS=EMP1*ETAB1*SBBYS
      M=3
      KK1=(ML-1)/M+1
      KK=KK1+1
      K=KK
      MK=M*(K-2)+1
      DSWCOS(LLIM)=PIMS
      RB(LLIM)=ETAB
      L1=LLIM
      COSSL=0.
      RS=1.+TWEM+AEP
      XW(KK)=1.
      COSSL(KK)=1./SQRT(1.+EMBF2)
      DO 8 LL=1,ML1
      L=LLIM-LL
      XL=X(L)
      XM=XL**EM
      DSWCOS(L)=PIMS*XM
      IF (BDYONLY) GO TO 8
      RB(L)=ETAB*XM
      IF (MK.NE.L) GO TO 8
      K1=K
      K=K-1
      MK=M*(K-2)+1
      XW(K)=XL
      XSE=.5*(XW(K1)+XL)
      TXSE(K)=XSE
      PTWP1(K)=PTOT2(RSE)
      DELR(K)=RSE-ETAB*XSE**EM
      RSK1=RS
      XM12=(XM/XL)**2
      RS=XM*(1.+(TWEM/SQRT(XL)+AEP)/XM12)
      COSSL(K)=1./SQRT(1.+EMBF2*XM12)
      DRM1S=EMETS*(RSK1-RS-RB(L1)+RB(L))
      DSWCSL(K,K)=DRM1S*.25*(COSSL(K)+COSSL(K1))
      L1=L
      DO 7 J=K1,KK
7     DSWCSL(J,K)=DRM1S*COSSL(J)
8     CONTINUE
      DSWCOS=PIMS*(.1*X(2))**EM
      IF (BDYONLY) GO TO 10
      XW=0.
      XSE=.5*XW(2)
      TXSE=XSE
      PTWP1=PTOT2(RSE)
      DELR=RSE-ETAB*XSE**EM
      DRM1S=EMETS*(RS-RB(L1))
      DSWCSL=DRM1S*.25*COSSL(2)
      DO 9 J=2,KK
9     DSWCSL(J,1)=DRM1S*COSSL(J)
      XL1=X(6)
      XL2=X(16)
      RL1=RB(6)
      RL2=RB(16)
C
C    ANGLE OF ATTACK VARIATION
C
      ANGO=DEL*(RB(ML)-ETAB)/(1.-X(ML))
10    PRINT DATA
      PRINT 36, HEAD
      NANG=NALF
      DO 28 I=1,NANG
      ANG=DTOR*ANGL(I)
      IF (NCASE-3) 12,11,11
```

```
C
C     WING UPPER SURFACE PRESSURE
11    IF (ANG) 14,15,17
12    SINE(I)=SIN(ANG)
      COSE(I)=SQRT(1.-SINE(I)**2)
      CA0=ABS(AMCH*ANG)
      IF (ANG) 13,15,16
13    GP1K04=GP14*CA0
      POS=1.+GAM*CA0*(GP1K04+SQRT(1.+GP1K04**2))
      PUPIQI(I)=PQ*(POS-1.)
      PRINT 23, ANGL(I),PUPIQI(I)
14    IF (ANGO.LE.ANG) GO TO 17
      NANG=NANG-1
      PRINT 35, ANGL(I)
      GO TO 28
15    DPSBYQS(I)=S1STBYS*PQLAM*PBBPOL(I)
      U2=1.
      IO=I
      EME=EM
      GO TO 21
16    POE=(1.-GM12*CA0)**ZGG1
      IF (POE.LT.0.) POE=0.
      PUPIQI(I)=PQ*(POE-1.)
      PRINT 22, ANGL(I),PUPIQI(I)
17    DPSBYQS(I)=S1STBYS*(PQLAM*PBBPOL(I)-PUPIQI(I))
C
C     EFFECTIVE BODY SHAPE DUE TO ANGLE OF ATTACK
      TN=SINE(I)/COSE(I)
      U2=1./(1.+F*TN)**2
      IF (FM.EQ.1) GO TO 20
      RHORAT=(RL2+XL2*TN)/(RL1+XL1*TN)
      IF (RHORAT) 19,19,18
18    EME=ALOG(RHORAT)/ALOG((XL2-RL2*TN)/(XL1-RL1*TN))
      IF (EME-.51) 19,21,21
19    EME=.51
      GO TO 21
20    EME=1.0
21    IF (EME-EMESAV) 22,23,22
22    EMESAV=EME
      CALL MTLUP (EME,YF,2,13,13,5,IP,VARI,VARD)
      ETRAT=ETABE*ETABI
      ETE1I=1./(1.-ETABE)
      EME2=EME*EME
      FRME=4.*EME
      FRME1=FRME-1.
      ZME=2.*EME
      ZMEM=ZME+EM
      THR2ME=3.-ZME
      EME1=EME-1.
      AI=AI1-AI2*EME1/(EME1-G37*FRME1)
      Z1ME=2.-ZME
      GME2I=GMI/EME2
      FOEM=FOE*EM
      FOEM1=EMP1*FOE
      DJETB=DJOE*ETE1I*ONETET
C
C     BODY AXIS COEFFICIENTS FROM INTEGRATED WING AND BODY PRESSURES
23    CAY=U2*ETRAT**2
      D2ME2K=DEL2*EME2/CAY
      D2MS=D2ME2K*SBBYS
      D2MS2=2.*D2MS
      D2MSC=-D2MS
      EE4U2=4.*U2*(ESAV*AI*ETABE*THR2ME/(EME2*SQRT(FOE*FRME1)))
      E4UM=EE4U2*ZMP1I
      EESAV=1./(ZMEM-1.)+E4UM
      EK=EPS*CAY
      F1EK=F1E*EK
      F1IK=F1I*EK
```

```
      EKGO=EK*GME2I
      EPSAVO=F1EK-PBPI*EKGO
      EPSAV1=F1EK-EKGO
      EPSAV2=ONETET*(EK*DJ1E*ETE1I-EKGO)
      CNB(I)=D2MS2*(FOEM1*EESAV+EPSAV1)
      CND(I)=D2MS2*FOEM1*EME*ETRAT*EE4U2/((ZME+1.)*THR2ME)
      CNW(I)=D2MS2*(EMP1*(DJETB*EESAV+ZG1ET*(EMSAV/(FRME1-ZMM1)+AEP/
     1 (ZME-EMM1))-EME*ETRAT*E4UM*FOE/THR2ME)+EPSAV2)
      CAP(I)=PI*D2MS*EMP1*FI*(FOEM*(1./(ZME+ZMM1)+EE4U2*EM4I)+.5*EPSAVO)
      CN(I)=CNB(I)+CND(I)+CNW(I)+DPSBYQS(I)
      CMN=D2MSC*EMP1*(EMP2*((FOE+DJETB)*(1./ZMEM+EE4U2*THM3I)+
     1 ZG1ET*(EMSAV/(FRME+THR2M)+AEP/(ZMEM-ZMM1)))+EPSAV1+EPSAV2)
      CMA=D2MSC*EM1M2F2*(FOEM*(1./(ZMEM+ZMM1)+EE4U2*SIXMI)+EPSAVO/3.)
      CMCG(I)=CMN+CMA-XSC*DPSBYQS+.5*EMP2*(CN(I)*XCG+CAP(I)*FI*YCG)
C
C    SKIN FRICTION ON BODY
      FOE=FOE
      E2U2=.5*EE4U2
      APC=GAM*EME2/EK
      AP=APO/PT2P1
      WING=.FALSE.
      CAFB2=CFCON*SKNFRC(X,LLIM,DSWCOS,GAM,ALAM,FUN1)
      IF (BDYONLY) GO TO 25
C
C    SKIN FRICTION ON WING UPPER AND LOWER SURFACES
      CAFU=CFOCR*(1.+CFDCFO1(I))
      CAFL=0.
      WING=.TRUE.
      DO 24 K=1,KK1
      K1=KK-K+1
      AP=APO/PTWP1(K)
      DLR=DELR(K)
      SAVXW=XW(K)
      XW(K)=TXSE(K)
      CAFL=CAFL+PTWP1(K)*SKNFRCW(XW(K),K1,DSWCSL(K,K),GAM,ALAM,FUN1)
 24   XW(K)=SAVXW
      CAFL=CAFLC*CAFL
      IF (XOUT) PRINT OUT
C
C    LIFT,  DRAG,  AND  L / D
      CAF(I)=CAFB2+CAFU+CAFL
      GO TO 26
 25   CAF(I)=2.*CAFB2
      CAP(I)=2.*CAP(I)
      CN=0.
      CMCG=0.
 26   CA(I)=CAP(I)+CAFACTR*CAF(I)
      CL(I)=CN(I)*COSE(I)-CA(I)*SINE(I)
      CD(I)=CA(I)*COSE(I)+CN(I)*SINE(I)
      CLCD(I)=CL(I)/CD(I)
      IF (CDMIN.LT.CD(I)) GO TO 27
      IMIN=I
      CDMIN=CD(I)
 27   IF (CLCD(I).LT.CLDMX) GO TO 28
      CLDMX=CLCD(I)
      IMAX=I
 28   CONTINUE
      IF (XOUT) PRINT 36, HEAD
      IF (NANG-3) 31,29,29
C
C    QUADRATIC INTERPOLATION OF DRAG POLAR TO GET  (L/D)MAX, ETC.
C
 29   IF (IMAX.LT.2) IMAX=2
      IF (IMAX.GE.NANG) IMAX=NANG-1
      IXP=IMAX+1
      IXM=IMAX-1
      Y1=CD(IXM)
      Y2=CD(IMAX)
```

```
      Y3=CD(IXP)
      X1=CL(IXM)
      X2=CL(IMAX)
      X3=CL(IXP)
      X12=X1-X2
      X23=X2-X3
      IF (IFMIN) GO TO 30
      X31=X3-X1
      A=(Y1*X23+Y2*X31+Y3*X12)/(-X12*X23*X31)
      XA=.5*(A*(X3+X1)-(Y3-Y1)/X31)
      XA2YAA=Y2+X2*(2.*XA-A*X2)
      CLMX2=XA2YAA/A
      IF (CLMX2.LT.0.) GO TO 30
      CLMX=SQRT(CLMX2)
      CDMX=2.*(XA2YAA-XA*CLMX)
      CLDMX=CLMX/CDMX
      CALL MTLUP (0.,CDALO,2,NANG,11,2,KP,CL,CDANGL)
      CALL MTLUP (CLMX,ALPHX,2,NANG,11,1,IMAX,CL,ANGL)
      IFMIN=.TRUE.
      IMAX=IMIN
      GO TO 29
30    Y3221=(Y3-Y2)/(Y2-Y1)
      X3221=X23/X12
      CLMN=.5*(Y3221*(X2+X1)-X3221*(X3+X2))/(Y3221-X3221)
      CALL MTLUP (CLMN,CDALN,2,NANG,11,2,KP,CL,CDANGL)
C
C     MAIN OUTPUTS
C
      PRINT 37, CLDMX,ALPHX,CLMX,CDMX,CDALO,CDALN,CLMN
      CALL SUMMARY (CLDMX,ALPHX,CLMX,CDALO,CDALN,CL(IO),HEAD,NCASE)
31    PRINT 34, (ANGL(I),CL(I),CD(I),CMCG(I),CLCD(I),CN(I),CNB(I),CND(I)
     1,CNW(I),DPSBYQS(I),CA(I),CAP(I),CAF(I),I=1,NANG)
      NCASE=4
      GO TO 1
32    CALL PRNTSUM (CLDMX,ALPHX,CLMX,CDALO,CDALN,CL(IO),HEAD,NCASE)
      STOP
C
33    FORMAT (F12.2,15H DEG.  PUPIQI =,F10.5)
34    FORMAT (//3X,5HALPHA,8X,2HCL,8X,2HCD,8X,2HCM,7X,3HL/D,9X,2HCN,8X,
     1 3HCNB,7X,3HCND,7X,3HCNW,6X,4HDP/Q,8X,2HCA,8X,3HCAP,7X,3HCAF//
     2 (F7.1,3X,3F10.5,F9.2,2X,5F10.5,X,3F10.5))
35    FORMAT (//F8.2,28H DEG., TOO NEGATIVE FOR BODY)
36    FORMAT (1H1/20X8A10/)
37    FORMAT (//11H (L/D)MAX =,F8.4,11H AT ALPHA =,F7.4,    26H DEGREES,
     1 WITH CL AND CD =,2F9.6//6H CDO =,F10.8,14H, AT ALPHA 0 =,F8.4//
     2 9H CD MIN =,F10.8,12H, AT ALPHA =,F8.4,9H AND CL =,F8.6)
38    FORMAT (8A10)
      END


      FUNCTION PTOT (RS)
C
C     TOTAL TO STATIC PRESSURE RATIO ACROSS SHOCK, AND SHOCK POSITION
C
      COMMON DUMB(16),XS,GAM,GM1,GM12,GP12,EM,EMI,EM32,ZMM,ZEMI1,THR2M,
     1 AMCH2,DEL,TWEM,AEP
C     X POSITION FOR GIVEN SHOCK RADIUS
      XSMO=RS
      X0=RS**EMI
      DO 1 I=1,10
      X01M=X0**EMI
      XSM=RS/(1.+(AEP+TWEM/SQRT(X01M))*(X01M/X0)**2)
      IF (XSM/XSMO.GT..999) GO TO 2
      X0=XSM**EMI
1     XSMO=XSM
```

```
2       XS=XSM**EMI
        GO TO 3
        ENTRY PTOT2
C     SHOCK RADIUS AT GIVEN X POSITION
        XSM=XS**EM
        RS=XSM+(AEP+TWEM/SQRT(XS))*XS*XS/XSM
3       XSL2M=XSM**2
        TTHX2=(DEL*(EM*XSL2M/XS+XS*ZMM*AEP+.5*THR2M*TWEM*SQRT(XS)))**2
        AM2=AMCH2*TTHX2/(XSL2M+TTHX2)
        AMG1=GP12*AM2*(1.+GM12*AMCH2)/(1.+GM12*AM2)
        AMG2=GP12/(GAM*AM2-GM12)
        PTOT=EXP((ALOG(AMG2)+GAM*ALOG(AMG1))/GM1)
        RETURN
        END


        FUNCTION SKNFRC (X,LLIM,DSWCOS,GAM,ALAM,FUN1)
C
C     LAMINAR, COMPRESSIBLE SKIN FRICTION              (DATA ARE FOR TW/TT = .41667)
C
        DIMENSION X(19), DSWCOS(19), XI(19), U(19), BETA(19), DCF(19),
       1 BIT(3), B(15), TTH2(30), THT2(2)
        EQUIVALENCE (FWPP,THT2(2))
        DATA B,TTH2/-.2,-.1,0.,.05,.1,.2,.3,.4,.5,.6,.8,1.,1.2,1.6,2.,
       1 .293,.2485,.2205,.2095,.1998,.1845,.1725,.1627,.1547,.1479,.137,
       2 .1285,.1218,.1116,.1107, .269,.387,.4696,.5051,.5373,.5944,.6447,
       3 .69,.73165,.7703,.8408,.9044,.9627,1.0677,1.1613/,          JP/11/
       4, GX1,GX2,ZGM1/-.2857142857143,1.285714285714,5./
C     BEGIN WITH  X(1) = 0., XI(1) = 0., BETA = .5  (BLUNT-NOSED BODY)
1       BETA(1)=.5
        TMPT2=.23209
        FPTH=.28779
        GO TO 2
        ENTRY SKNFRCW
C     BEGIN WITH  X(1) = XSE, XI(1) = 0., BETA = 0.  (UNDERSIDE OF WING)
        BETA=0.
        TMPT2=.441
        FPTH=.22052
2       XM=X+.1*(X(2)-X)
        PEPT2=P(XM)
        UM=SQRT(ZGM1*(PEPT2**GX1-1.))
        CALL MGAUSS (X,XM,1,XIM,FUN1,FOFX,1)
        XIM=ALAM*XIM
        TH2UR=TMPT2*XIM
        DCF(1)=PEPT2**GX2*FPTH*DSWCOS(1)*SQRT(UM**3/TH2UR)
        XI(1)=XIM
        U(1)=UM
        DO 9 IP=2,LLIM
        XP=X(IP)
        CALL MGAUSS (XM,XP,1,DXI,FUN1,FOFX,1)
        DXI=ALAM*DXI
        XI(IP)=DXI+XIM
        PEPT2=P(XP)
        U(IP)=SQRT(ZGM1*(PEPT2**GX1-1.))
        ALNUR=ALOG(U(IP)/UM)
        ALNUR2=2.*ALNUR
        DXIUTH=DXI/TH2UR
        RLAM=7.7809*(U(IP)/UM-1.)/DXIUTH
        BET=RLAM*(1.+(RLAM-1.)*((.0206737*DXIUTH-.20419)*DXIUTH+.344145))
        KK=1
        K1=0
C      ITERATION FOR BETA  (LOCAL VELOCITY-VARIATION PARAMETER)
        DO 7 J=1,29
        BITR=BET
        BIT(KK)=BET
        IF (KK-3) 5,3,3
```

```
3       KK=1
        B32=BIT(3)-BIT(2)
        B21=BIT(2)-BIT(1)
        IF (ABS(B21+B32).LT.ABS(B32)) GO TO 4
        BDENOM=B32-B21
        IF (BDENOM.EQ.0.) GO TO 6
        BET=(BIT(1)*BIT(3)-BIT(2)**2)/BDENOM
        K1=0
        GO TO 6
4       BET=(BIT(2)+BIT(3))/2.
        GO TO 6
5       KK=KK+K1
        K1=1
6       IF (BET.GT.2.) BET=1.4
        CALL MTLUP (BET,THT2,2,15,15,1,JP,B,TTH2)
        BET=ALNUP2/(ALNUP+ALOG(1.+DXIUTH*(2.-BET)*THT2))
        IF (ABS(BET/BITR-1.)-.0001) 8,8,7
7       CONTINUE
        PRINT 11, XP,BITR,BET
8       BETA(IP)=BET
        CALL MTLUP (BET,THT2,2,15,15,2,JP,B,TTH2)
        TH2UP=(1.+DXIUTH*(2.-BET)*THT2)*TH2UR
        DCF(IP)=PEPT2**GX2*FWPP*DSWCOS(IP)*SQRT(U(IP)**3*THT2/TH2UR)
        XM=XP
        XIM=XI(IP)
9       UM=U(IP)
        IF (LLIM.EQ.2) GO TO 10
        SKNFRC=SUM(X,DCF,LLIM)
        RETURN
10      SKNFRC=.5*(DCF+DCF(2))*(X(2)-X)
        RETURN
C
11      FORMAT (/26H BETA UNCONVERGED AT X/L =,F8.5,12H BETA VALUES,2F12.8
       1)
        END

        SUBROUTINE FUN1 (X,FOFX)
C
C    INTEGRAND OF STEWARDSON TRANSFORMATION INTEGRAL FOR SKIN FRICTION
C
        COMMON AP,Z1ME,E2U2,FOE,F1EK,THG12G,TWM,EMBF2,D2ME2K,X2M,WING
        LOGICAL WING
        X2M=X**TWM
        X2=X*X
        IF (WING) 2,1
1       XF=X2M
        X2=1./(X2*X2M)
        GO TO 3
2       XF=1.
        X2=X2M/X2
3       FOFX=P2(X)**THG12G*XF*SQRT(1.+EMBF2*X2)
        RETURN
        END


        FUNCTION P (X)
C
C    BODY OR WING SURFACE PRESSURE
C
        COMMON AP,Z1ME,E2U2,FOE,F1EK,THG12G,TWM,EMBF2,D2ME2K,X2M,WING,F01,
       1F11K,DLR,ETB,ONETB,DUMB(13),TWEM,AEP
        LOGICAL WING
        X2M=X**TWM
        ENTRY P2
        IF (WING) 2,1
1       FTOE=FOE
        FT1EK=F1EK
        GO TO 3
```

```
2       XM=SQRT(X2M)
        ETR=(((DLR+ETB*XM)/(XM+(TWEM*SQRT(X)+AEP*X)*X/XM)-ETB)*ONETB)**2
        FTOE=FOE+ETR*(F01-FOE)
        FT1EK=F1EK+ETR*(F11K-F1EK)
3       X21ME=X**Z1ME
        P=AP*((1.+E2U2*X21ME/SQRT(X))*FTOE/(X21ME+D2ME2K)+FT1EK)
        IF (P.LT.1) RETURN
        PRINT 4, P,X,E2U2,D2ME2K,ETR,FTOE,FT1EK
        P=.9999999925
        RETURN
C
4       FORMAT (4H P =,F13.5,16H SET = 1. AT X =,F10.5,10X,5E13.5)
        END


        FUNCTION SUM(X,Y,N)
C
C     TRAPEZOIDAL INTEGRATION FOR UNEQUAL INTERVALS
C
        DIMENSION X(19),Y(19)
        M=N-1
        PSUM=Y*(X(2)-X)+Y(N)*(X(N)-X(M))
        DO 1 I=2,M
1        PSUM=PSUM+Y(I)*(X(I+1)-X(I-1))
        SUM=.5*PSUM
        RETURN
        END


        SUBROUTINE SUMMARY(A,B,C,D,E,F,H,N)
C
C     COLLECTION OF SUMMARY RESULTS ON A FILE (TAPE7) FOR SEPARATE OUTPUT
C
        DIMENSION D(2), E(2), H(8), L(25), O(14,25)
        DATA L,I,SKIP/26*0,3H(/)/
        IF (N-3) 1,2,3
1       IF (L(1).EQ.1) GO TO 6
        I=0
2       L(I+1)=1
3       I=I+1
        O(1,I)=A
        O(2,I)=B
        O(3,I)=C
        O(4,I)=D
        O(5,I)=D(2)
        O(6,I)=E
        O(7,I)=E(2)
        O(8,I)=F
        O(9,I)=H(3)
        O(10,I)=H(4)
        O(11,I)=H(5)
        O(12,I)=H(6)
        O(13,I)=H(7)
        O(14,I)=H(8)
        IF (I.LT.25) RETURN
        ENTRY PRNTSUM
6       WRITE(7,9)
        DO 7 J=1,I
        IF (L(J).EQ.1) WRITE(7,SKIP)
        WRITE(7,8) (O(K,J),K=1,14)
7       L(J)=0
        I=0
        IF (N.LT.3) GO TO 2
        RETURN
8       FORMAT(X2F9.4,F8.5,F9.5,F8.2,F9.4,F8.2,F8.5,3X,6A10)
9       FORMAT(1H1/16H HYPAERO SUMMARY//3X,5H(L/D),5X,5HALPHA,4X,2HCL,3X,
       1 2(5X,2HCD,5X,5HALPHA),4X,2HCL/7X,3HMAX,2X,2(3X,5HL/DMX),
       2 2(6X,1H0,3X),2(2X,3HMIN,4X),3HA=0)
        END
```

Input

A single case consists of the determination of the aerodynamic coefficients over a given set of angles of attack. The first card for each case provides a heading for the printout; it consists of 80 columns of any desired FORTRAN characters. The remaining cards for each case are interpreted by a system loading subroutine (NAMELIST) which is very flexible. The data block begins with an arbitrary name ($DATA in the present case) and ends with the dollar sign ($); the variables between may be in any order and need appear only if values are to be different from those preassigned or used in the previous case of the same computer run. Column one of all these cards is blank. A description of the input FORTRAN variables with their correct type and preassigned values (if any) in parentheses is as follows:

FORTRAN variable	Description
TINF	free-stream static temperature, T_∞, $^{\circ}R$ (real)
AMCH	free-stream Mach number, M_∞ (real)
NALF	number of angles of attack, maximum of 11 (integer)
ANGL	angle-of-attack array, decreasing order, deg (real)
EM	power-law exponent, m (real)
F	body fineness parameter, f (real)
REL	Reynolds number based on body length, $R_{\infty,l}$ (real)
SSB	ratio of reference area for coefficients to body planform area; if zero, program uses wing planform area (real;0.)
XCG	ratio of x location of moment reference center to body length (real)
YCG	ratio of y location of moment reference center to maximum body radius (real)

FORTRAN variable	Description
PBPI	ratio of base pressure to free-stream static pressure (real;1.)
CAFCTR	multiplication factor times calculated laminar skin friction (real;1.)
XOUT	extra output at each angle of attack if XOUT = .TRUE.(logical,.FALSE.)
PBBP0L	array of NALF values of wing upper surface pressure parameter $\left(\dfrac{\bar{P} - P_0}{\lambda_{cr}} \text{ in ref. 20}\right)$ corresponding to angles of attack ANGL (real)
CFDCF01	array of NALF values of wing skin-friction parameter $\left(\dfrac{C_{F,\Delta}}{C_{F,0,cr}} - 1 \text{ in ref. 20}\right)$ corresponding to angles of attack ANGL (real)
BDYONLY	set equal to .TRUE. for axisymmetric body only, .FALSE. for half body with wing (logical; .FALSE.)
NCASE	indicator for each additional case of a run to avoid unnecessary recomputations (integer; 1 initially, 4 each case thereafter). After first case of a run set NCASE = 2 if AMCH or TINF is changed; set NCASE = 3 if EM is changed but AMCH and TINF are not; for no change to AMCH, TINF or EM use preassigned value 4.

Output

There are four possible output blocks for each case, only two of which always appear. First comes the input list with four added variables. These are GAM, the ratio of specific heats γ; ALAMCR, a parameter (λ_{cr}) from reference 20; DEL, the slender body parameter δ; and EPS, the shock strength parameter ϵ_1. Next is a list of the angles of attack with the pressure coefficient, Mach number and sine squared of the shock angle for oblique shock, and with the pressure coefficient and Mach number for Prandtl-Meyer expansion through the angle (appears only for new Mach numbers). Third is a list of variables used in the angle-of-attack and skin-friction calculations, which appears only if called by setting XOUT = .TRUE. in the input list. Fourth is the standard output of stability-axis and body-axis coefficients with the interpolated $(L/D)_{max}$. The normal-force coefficient is also broken down into contributions from the body CNB, the body boundary-layer area under the wing CND, the rest of the under-wing area CNW, and the wing upper surface DP/Q. The axial force is broken into the contribution from the pressure CAP and from the skin friction CAF. In addition to these results, after all cases have been run, a summary of results is printed out for cases with angles of attack.

Example

Input cards for a run of two sample cases are presented below. The first case is for the complete configuration with $m = 0.75$, $f = 7$, at $M_\infty = 12$, $R_{\infty,l} = 256.26 \times 10^6$ and 11 angles of attack. The second is for the axisymmetric body having the same parameters.

```
POWER-LAW TRANSPORBITER  MACH 12  EM=.7500  F=7.00  REY=4.42E6/M  PBASE=PINFINIT
 $DATA AMCH=12.,EM=.75,F=7.,REL=256.26E6,TINF=408.,XCG=.6,YCG=.15,
 PBBPOL=2.86,3.19,3.52,3.71,3.9,4.09,4.27,4.62,4.95,5.24,5.5,
 CFDCF01=-.07,.06,.23,.32,.42,.52,.62,.84,1.09,1.35,1.59,
 NALF=11,ANGL=3.,2.,1.,.5,0.,-.5,-1.,-2.,-3.,-4.,-5.$
POWER-LAW BODY OF REVOL   MACH 12  EM=.7500  F=7.00  REY=4.42E6/M  PBASE=PINFINIT
 $DATA NCASE=2,BODYONLY=.TRUE.,NALF=1,ANGL(1)=0.,PBBPOL=0.,CFDCF01=0.$
```

The output for these input cards is shown below. The total computation time on a CDC 6600 series computer at the Langley Research Center was less than 15 seconds (excluding compilation).

```
$DATA

NCASE   =  1,

GAM     =  0.14E+01,

TINF    =  0.408E+03,

AMCH    =  0.12E+02,

NALF    =  11,

ANGL    =  0.3E+01,  0.2E+01,  0.1E+01,  0.5E+00,  0.0, -0.5E+00, -0.1E+01,
          -0.2E+01, -0.3E+01, -0.4E+01, -0.5E+01,

EM      =  0.75E+00,

F       =  0.7E+01,

REL     =  0.25626E+09,

SSB     =  0.0,

XCG     =  0.6E+00,

YCG     =  0.15E+00,

PBPT    =  0.1E+01,

CAFACTR =  0.1E+01,

ANGO    = -0.11176877154745E+00,

XCUT    = F,
```

```
PBBPOL  =  0.286E+01,  0.319E+01,  0.352E+01,  0.371E+01,  0.39E+01,
           0.409E+01,  0.427E+01,  0.462E+01,  0.495E+01,  0.524E+01,
           0.55E+01,

CFDCF01 = -0.7E-01,  0.6E-01,  0.23E+00,  0.32E+00,  0.42E+00,  0.52E+00,
           0.62E+00,  0.84E+00,  0.109E+01,  0.135E+01,  0.159E+01,

ALAMCR  =  0.91969221746557E-02,

BDYONLY = F,

DEI     =  0.16325224594277E+00,

EPS     =  0.26056685930625E+00,

XSE     =  0.45E-02,

$END
```

```
                 POWER-LAW TRANSPORTER  MACH 12  EM=.7500  F=7.00  REY=4.42E6/M  PBASE=PINFINIT

        3.00 DEG.  PUPTOT =   -.00605
        2.00 DEG.  PUPTOT =   -.00454
        1.00 DEG.  PUPTOT =   -.00257
         .50 DEG.  PUPTOT =   -.00137
        -.50 DEG.  PUPTOT =    .00155
       -1.00 DEG.  PUPTOT =    .00320
       -2.00 DEG.  PUPTOT =    .00746
       -3.00 DEG.  PUPTOT =    .01262
       -4.00 DEG.  PUPTOT =    .01887
       -5.00 DEG.  PUPTOT =    .02632

(L/D)MAX =  5.8468 AT ALPHA = -.0225 DEGREES, WITH CL AND CD =  .034100  .005832

CDO = .00282901, AT ALPHA O = -3.3873

CD MIN = .00282559, AT ALPHA = -3.4960 AND CL =-.001197
```

ALPHA	CL	CD	CM	L/D	CN	CNB	CNO	CNW	DP/Q	CA	CAP	CAF
3.0	.06419	.01308	.00211	4.91	.06478	.04397	.00011	.01492	.00578	.00970	.00926	.00043
2.0	.05418	.01021	.00024	5.30	.05450	.03764	.00011	.01250	.00425	.00832	.00790	.00042
1.0	.04424	.00781	-.00192	5.66	.04437	.03174	.00011	.01027	.00225	.00704	.00663	.00040
.5	.03928	.00678	-.00314	5.79	.03934	.02897	.00011	.00923	.00103	.00644	.00604	.00040
0.0	.03432	.00587	-.00447	5.85	.03432	.02632	.00011	.00825	-.00036	.00587	.00548	.00039
-.5	.02925	.00507	-.00593	5.78	.02931	.02381	.00011	.00731	-.00192	.00533	.00495	.00039
-1.0	.02436	.00440	-.00754	5.54	.02428	.02142	.00011	.00644	-.00369	.00482	.00444	.00038
-2.0	.01428	.00340	-.01125	4.20	.01415	.01708	.00011	.00484	-.00788	.00389	.00352	.00037
-3.0	.00400	.00289	-.01572	1.38	.00384	.01332	.00011	.00347	-.01307	.00310	.00273	.00036
-4.0	-.00654	.00289	-.02105	-2.26	-.00672	.01018	.00011	.00234	-.01935	.00243	.00207	.00036
-5.0	-.01737	.00343	-.02731	-5.06	-.01760	.00767	.00011	.00144	-.02682	.00190	.00155	.00035

```
$DATA

NCASE   =  2,

GAM     =  0.14E+01,

TINF    =  0.408E+03,

AMCH    =  0.12E+02,

NALE    =  1,

ANGL    =  0.0,  0.2E+01,  0.1E+01,  0.5E+00,  0.0, -0.5E+00, -0.1E+01,
          -0.2E+01, -0.3E+01, -0.4E+01, -0.5E+01,

EM      =  0.75E+00,

F       =  0.7E+01,

REL     =  0.25626E+09,

SSB     =  0.0,

XCG     =  0.65E+00,

YCG     =  0.15E+00,

PBPI    =  0.1E+01,

CAFACTR =  0.1E+01,

ANGO    = -0.11176877154745E+00,

XCUT    = F,

PBBPOL  =  0.0,  0.319E+01,  0.352E+01,  0.371E+01,  0.39E+01,  0.409E+01,
           0.427E+01,  0.462E+01,  0.495E+01,  0.524E+01,  0.55E+01,

CFDCF01 =  0.0,  0.6E-01,  0.23E+00,  0.32E+00,  0.42E+00,  0.52E+00,
           0.62E+00,  0.84E+00,  0.109E+01,  0.135E+01,  0.159E+01,
```

```
ALAMCR   =  0.91969221746557E-02,
BDYONLY  =  T,
DEL      =  0.16325224594277E+00,
EPS      =  0.26056685930625E+00,
XSE      =  0.13996004141169E-02,
$END
```

POWER-LAW BODY OF REVOL MACH 12 EM=.7500 F=7.00 REY=4.42E6/M PBASE=PINFINIT

ALPHA	CL	CD	CM	L/D	CN	CNB	CND	CNW	DP/Q	CA	CAP	CAF
0.0	0.00000	.01128	0.00000	0.00	0.00000	.07632	.00011	.00825	0.00000	.01128	.01096	.00032

HYPAERO SUMMARY

(L/D) MAX	ALPHA L/DMX	CL L/DMX	CD 0	ALPHA 0	CD MIN	ALPHA MIN	CL A=0	
5.8468	-.0225	.03410	.00283	-3.38	.0028	-3.50	.03432	TER MACH 12 EM=.7500 F=7.00 REY=4.42E6/M PBASE=PINFINIT

COMPUTER PROGRAM FOR CALCULATING K_0 AND λ_{cr}

The main program requires as inputs values of two parameters describing wing upper surface conditions. These values are an average wing upper surface pressure parameter (PBBP0L) and an average wing upper surface skin-friction parameter (CFDCF01). They are plotted in reference 20 (figs. 4 and 11 of the reference, respectively) as $\frac{\bar{\bar{P}} - P_0}{\lambda_{cr}}$ and $\frac{C_{F,\Delta}}{C_{F,0,cr}} - 1$ for delta wings as functions of λ_{cr} (a viscous interaction parameter) and K_0 ($= -M_\infty\alpha$). This program calculates K_0 for each angle of attack and the value of λ_{cr} for the delta wing corresponding to the power-law wing. As mentioned in the main body of the paper, the correspondence is based on the viscous effects, which are assumed to be approximately equal for wings with equal spans and equal values of $\iint x^{-1/2}\,dr\,dx$. For the power-law wings, this integral involves gamma functions which are approximated analytically in the program.

```
      PROGRAM UPPRESS(INPUT=201,OUTPUT=201,TAPE1=INPUT)
      DIMENSION ANGL(11), CAO(11), PO(11), HEAD(8), PBBPOL(11)
      NAMELIST /DATA/ REL,F,AMCH,TINF,EM,ETAB,FO,A1,NCASE,NALF,ANGL,XCG,
     1SSB,YCG
      DATA GAM,TWTT,PIF,ASAV/1.4,.41667,2.65868,0./
      GM1=GAM-1.
      GM1I=1./GM1
      GM83=GAM*8./3.
      GM12=.5*GM1
      GP14=(GAM+1.)/4.
      ZGG1=GAM/GM12
1     READ 11, HEAD
      IF (ENDFILE 1) 9,2
2     READ DATA
      IF (ANGL.EQ.ASAV) GO TO 7
      ASAV=ANGL
      DO 6 I=1,NALF
      ANG=.0174533*ANGL(I)
      CAO(I)=-AMCH*ANG
```

```
      IF (CAO(I)) 4,5,3
3     GP1K04=GP14*CAO(I)
      RTGK4=SQRT(1.+GP1K04**2)
      PO(I)=1.+GAM*CAO(I)*(GP1K04+RTGK4)
      PBBPOL(I)=GM83*(RTGK4+GP1K04*(2.+GP1K04/RTGK4))/SQRT(PO(I))
      GO TO 6
4     GM12K=1.+GM12*CAO(I)
      PO(I)=GM12K**ZGG1
      IF (PO(I).LT.0.) PO(I)=0.
      PBBPOL(I)=GM83*GM12K**GM1I
      GO TO 6
5     PO(I)=1.
      PBBPOL(I)=GM83
6     CONTINUE
7     ZM=2.*EM
      PRINT 12, HEAD
      IF (EM.EQ.BSAV) GO TO 8
      BSAV=EM
      EMM1=EM-1.
      EM41=4.*EM-1.
      EM4019=.4019*EM
      EMX1=1.5303-EM4019
      EMX2=.5/(.9274+EM4019)
      AT=.9775-.7627*EMM1/(EMM1+1.295*EM41)
      EMG=GM1*AT*ETAB/(EM*SQRT(2.*GAM*EM41*F0))
8     AEP=A1*(ETAB*F/AMCH)**2
      AEPX=AEP*EMX1/(5.-ZM)
      TTBTI=1.+GM12*AMCH*AMCH
      TWTI=TWTT*TTBTI
      TPTI=.273+(.195+.532*TWTT)*TTBTI
      SUTHI=198.6/TINF
      C1=(1.+SUTHI)/(TWTI+SUTHI)*SQRT(TWTI)
      C3=(1.+SUTHI)/(TPTI+SUTHI)*SQRT(TPTI)
      ZEM32=EMG*AMCH*F*F*SQRT(C1/REL)
      EM32X=.5*ZEM32/EMX1
      G2MRC=.69053*GM12*(AMCH**3)*SQRT(C3/REL)
      CREL=PIF*(EMX2+AEPX+EM32X)/(1.+AEP+ZEM32)
      ALAMCR=G2MRC/SQRT(CREL)
      PRINT 10, EM,F,AMCH,CREL,ALAMCR,(ANGL(I),CAO(I),PO(I),PBBPOL(I),I=
     11,NALF)
      GO TO 1
9     STOP
C
10    FORMAT (///15X,2HEM,9X,1HF,8X,4HMACH,6X,5HCRE/L,7X,11H(LAMBDA)CRE/
     1/9X,F10.4,2F10.2,F12.6,E17.6///6X,5HANGLE,6X,4H(K)0,7X,4H(P)0,7X,6
     2HLAM=0.,9X,13H(P-PO)/LAMBDA,6X,11H(CFD/CF0)-1//(F11.2,F11.4,2F11.5
     3))
11    FORMAT (8A10)
12    FORMAT (1H1,5X8A10)
      END
```

Input

A single case consists of calculations for a single configuration over a set of angles of attack. The first card is a heading consisting of any 80 FORTRAN characters. The remaining cards use the same loading subroutine as does the main program; the data block begins with $DATA and ends with $. The necessary input variables are TINF, AMCH, NANG, ANGL, EM, F, REL, ETAB, F0, and A1. Of these the first seven are the same as for the main program and the last three are from the similarity solution results.

See figure 3 and table I where ETAB = η_b, F0 = $F_0(\eta_b)$, and A1 = a_1. The program is set up so that the input cards to the main program may be used with these three variables added. Here is the input for the first sample case given with the main program:

```
POWER-LAW TRANSPORBITER  MACH 12  EM=.7500  F=7.00  REY=4.42E6/M   ***** UPPRESS
 $DATA AMCH=12.,EM=.75,F=7.,REL=256.26E6,TINF=408.,XCG=.6,YCG=.15,
 ETAB=.87507,F0=.69806,A1=.80732,
 NALF=11,ANGL=3.,2.,1.,.5,0.,-.5,-1.,-2.,-3.,-4.,-5.,$
```

Output

The output for the same case is shown in this section. In it (LAMBDA)CRE = λ_{cr} and (K)0 = K_0 are needed for use with reference 20. Also printed are the length ratio of the delta to the power-law wing, CRE/L; the ratio of inviscid surface pressure to free-stream static pressure, P0; and the average pressure parameter for $\lambda = 0$, LAM = 0. This latter value is a useful aid sometimes in interpolating values from the figures of reference 20.

```
POWER-LAW TRANSPORBITER  MACH 12  EM=.7500  F=7.00  REY=4.42E6/M   ***** UPPRESS
```

EM	F	MACH	CRE/L	(LAMBDA)CRE
.7500	7.00	12.00	1.056144	9.196840E-03

ANGLE	(K)0	(P)0	LAM=0.	(P-P0)/LAMBDA	(CFD/CF0)-1
3.00	-.6283	.39062	2.66866		
2.00	-.4189	.54202	2.99986		
1.00	-.2094	.74116	3.35458		
.50	-.1047	.86229	3.54092		
0.00	-0.0000	1.00000	3.73333		
-.50	.1047	1.15611	3.92899		
-1.00	.2094	1.33237	4.12332		
-2.00	.4189	1.75205	4.49871		
-3.00	.6283	2.27170	4.84414		
-4.00	.8378	2.90224	5.15051		
-5.00	1.0472	3.65262	5.41472		

REFERENCES

1. Eggers, A. J., Jr.; and Syvertson, Clarence A.: Aircraft Configurations Developing High Lift-Drag Ratios at High Supersonic Speeds. NACA RM A55L05, 1956.
2. Savin, Raymond C.: Approximate Solutions for the Flow About Flat-Top Wing-Body Configurations at High Supersonic Speeds. NACA RM A58F02, 1958.
3. Mandl, Paul: A Theoretical Study of the Inviscid Hypersonic Flow About a Conical Flat-Top Wing-Body Combination. AIAA J., vol. 2, no. 11, Nov. 1964, pp. 1956-1964.
4. Fetterman, David E.; Henderson, Arthur, Jr.; Bertram, Mitchel H.; and Johnston, Patrick J., Jr.: Studies Relating to the Attainment of High Lift-Drag Ratios at Hypersonic Speeds. NASA TN D-2956, 1965.
5. Becker, John V.: Studies of High Lift Drag Ratio Hypersonic Configurations. Proceedings of the Fourth Congress of the International Council of the Aeronautical Sciences, Robert R. Dexter, ed., Spartan Books, Inc., 1965, pp. 877-910.
6. Fetterman, David E.: Favorable Interference Effects on Maximum Lift-Drag Ratios of Half-Cone Delta-Wing Configurations at Mach 6.86. NASA TN D-2942, 1965.
7. Johnston, Patrick J.; Snyder, Curtis D.; and Witcofski, Robert D.: Maximum Lift-Drag Ratios of Delta-Wing—Half-Cone Combinations at a Mach Number of 20 in Helium. NASA TN D-2762, 1965.
8. Eggers, A. J., Jr.; Resnikoff, Meyer M.; and Dennis, David H.: Bodies of Revolution Having Minimum Drag at High Supersonic Airspeeds. NACA Rep. 1306, 1957. (Supersedes NACA TN 3666.)
9. Miele, Angelo; and Cole, Julian: Optimum Slender Bodies in Hypersonic Flow With a Variable Friction Coefficient. AIAA J., vol. 1, no. 10, Oct. 1963, pp. 2289-2293.
10. Miele, Angelo: A Study of the Slender Body of Revolution of Minimum Drag Using the Newton Busemann Pressure Coefficient Law. Tech. Rep. No. 62 (Doc. D1-82-0186), Boeing Scientific Res. Lab., Aug. 1962.
11. Peckham, D. H.: Measurements of Pressure Distribution and Shock-Wave Shape on Power-Law Bodies at a Mach Number of 6.85. Tech. Rep. No. 65075, British R.A.E., Apr. 1965.
12. Love, E. S.; Woods, W. C.; Rainey, R. W.; and Ashby, G. C., Jr.: Some Topics in Hypersonic Body Shaping. AIAA Paper No. 69-181, Jan. 1969.
13. Lees, Lester; and Kubota, Toshi: Inviscid Hypersonic Flow Over Blunt-Nosed Slender Bodies. J. Aeron. Sci., vol. 24, no. 3, Mar. 1957, pp. 195-202.

14. Kubota, Toshi: Investigation of Flow Around Simple Bodies in Hypersonic Flow. GALCIT Memo No. 40 (Contract No. DA-04-495-Ord-19), June 25, 1957.

15. Mirels, Harold: Hypersonic Flow Over Slender Bodies Associated With Power-Law Shocks. Vol. 7 of Advances in Applied Mechanics, H. L. Dryden and Th. von Kârmân, eds., Academic Press, Inc., 1962.

16. Mirels, Harold: Approximate Analytic Solutions for Hypersonic Flow Over Slender Power Law Bodies. NASA TR R-15, 1959.

17. Lees, Lester: Laminar Heat Transfer Over Blunt-Nosed Bodies at Hypersonic Flight Speeds. Jet Propulsion, vol. 26, no. 4, Apr. 1956, pp. 259-269, 274.

18. Smith, A. M. O.: Rapid Laminar Boundary-Layer Calculations by Piecewise Application of Similar Solutions. J. Aeron. Sci., vol. 23, no. 10, Oct. 1956, pp. 901-912.

19. Cohen, Clarence B.; and Reshotko, Eli: Similar Solutions for the Compressible Laminar Boundary Layer With Heat Transfer and Pressure Gradient. NACA Rep. 1293, 1956. (Supersedes NACA TN 3325.)

20. Bertram, Mitchel H.: Hypersonic Laminar Viscous Interaction Effects on the Aerodynamics of Two-Dimensional Wedge and Triangular Planform Wings. NASA TN D-3523, 1966.

21. Spencer, Bernard, Jr.; and Fox, Charles H., Jr.: Hypersonic Aerodynamic Performance of Minimum-Wave-Drag Bodies. NASA TR R-250, 1966.

22. Hayes, Wallace D.; and Probstein, Ronald F.: Hypersonic Flow Theory. Vol. I – Inviscid Flows. Second ed., Academic Press, Inc., 1966.

23. Townsend, James C.: Aerodynamic Interference Effects on Half-Cone Bodies With Thin Wings at Mach 10.03. NASA TN D-5898, 1970.

24. Anon.: U.S. Standard Atmosphere, 1962. NASA, U.S. Air Force, and U.S. Weather Bur., Dec. 1962.

25. McCracken, Daniel D.: A Guide to FORTRAN Programming. John Wiley & Sons, Inc., c.1961.

TABLE I.- SOLUTIONS TO THE HYPERSONIC SIMILARITY EQUATIONS
FOR POWER-LAW BODIES OF REVOLUTION

m	η_b	$F_0(\eta_b)$	$F_1(\eta_b)$	J_0	J_1	a_1
$\gamma = 7/5$						
1.00000	0.91492	0.87342	0.9179	0.07323	0.08410	0.47546
.95000	.91034	.84711	1.0591	.07589	.09551	.52709
.90000	.90465	.81630	1.2306	.07909	.11044	.58604
.85000	.89743	.78174	1.4386	.08303	.13067	.65291
.80000	.88798	.74265	1.6887	.08799	.15918	.72741
.75000	.87507	.69806	1.9811	.09444	.20098	.80732
.70000	.85648	.64662	2.2986	.10318	.26459	.88631
.66667	.83880	.60763	2.4964	.11098	.32565	.93216
.63333	.81391	.56403	2.6392	.12129	.40794	.96566
.60000	.77647	.51478	2.6593	.13564	.51763	.98034
.55000	.66414	.42678	2.2510	.17318	.74598	.96791
.53000	.56901	.38500	1.8876	.20119	.86687	.96377
.51000	.37221	.33757	1.4110	.25443	1.04110	.97539
.50500	.27299	.32450	1.2766	.28069	1.11845	.98249
.50000	.00000	.31077	1.1366	.35808	1.36841	.99182
$\gamma = 5/3$						
1.00000	0.87041	0.81065	0.7836	0.10244	0.10987	0.46531
.95000	.86429	.78363	.9017	.10532	.12597	.51356
.90000	.85679	.75282	1.0433	.10872	.14660	.56788
.85000	.84740	.71823	1.2122	.11283	.17364	.62833
.80000	.83532	.67912	1.4108	.11787	.20994	.69402
.75000	.81919	.63448	1.6356	.12422	.25974	.76228
.70000	.79658	.58296	1.8685	.13248	.32919	.82727
.66667	.77569	.54389	2.0053	.13956	.39031	.86398
.63333	.74719	.50016	2.0956	.14850	.46626	.89116
.60000	.70595	.45067	2.0942	.16025	.55904	.90627
.55000	.59076	.36177	1.7872	.18792	.73266	.91473
.53000	.49985	.31912	1.5217	.20647	.81845	.92427
.51000	.32217	.26988	1.1590	.23916	.93877	.94825
.50500	.23542	.25600	1.0506	.25495	.99164	.95764
.50000	.00000	.24113	.9315	.30378	1.16431	.96872

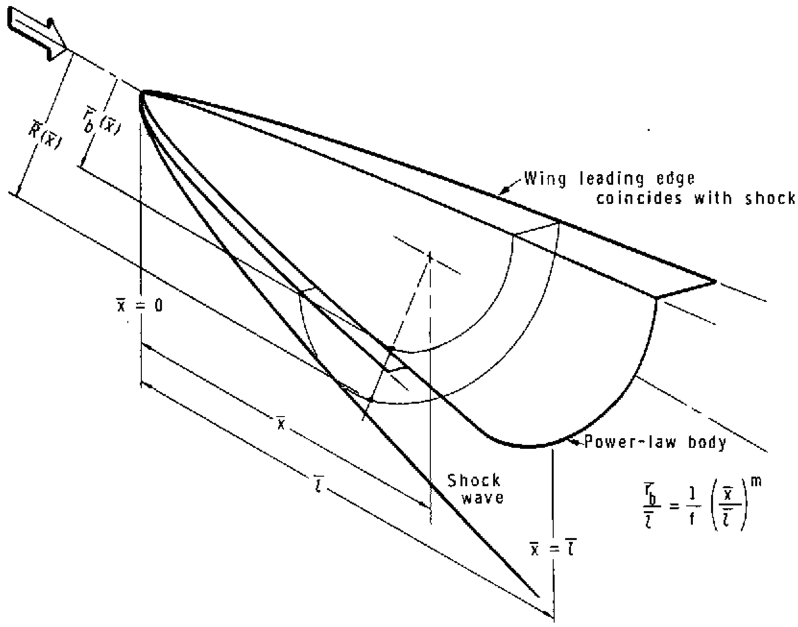

(a) General power-law, wing-body configuration.

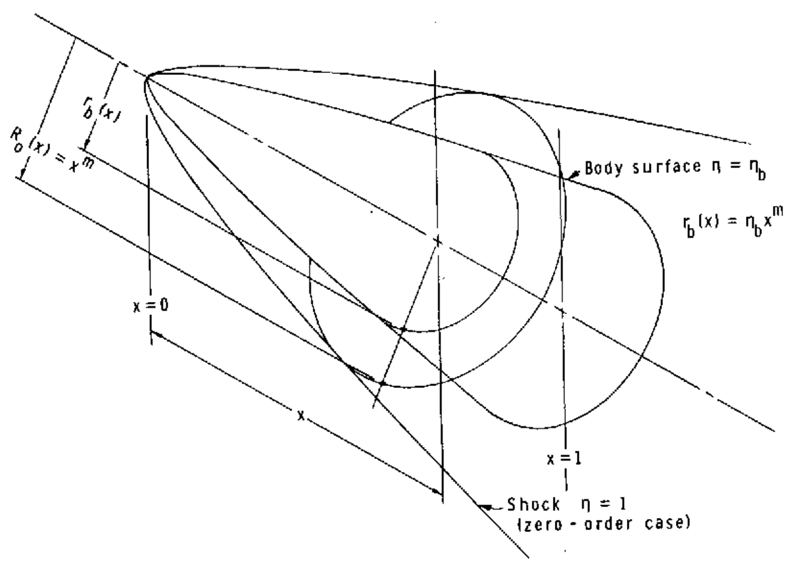

(b) Body of revolution in nondimensional coordinates.

Figure 1.- Configuration studied, showing relation between physical and nondimensional coordinates.

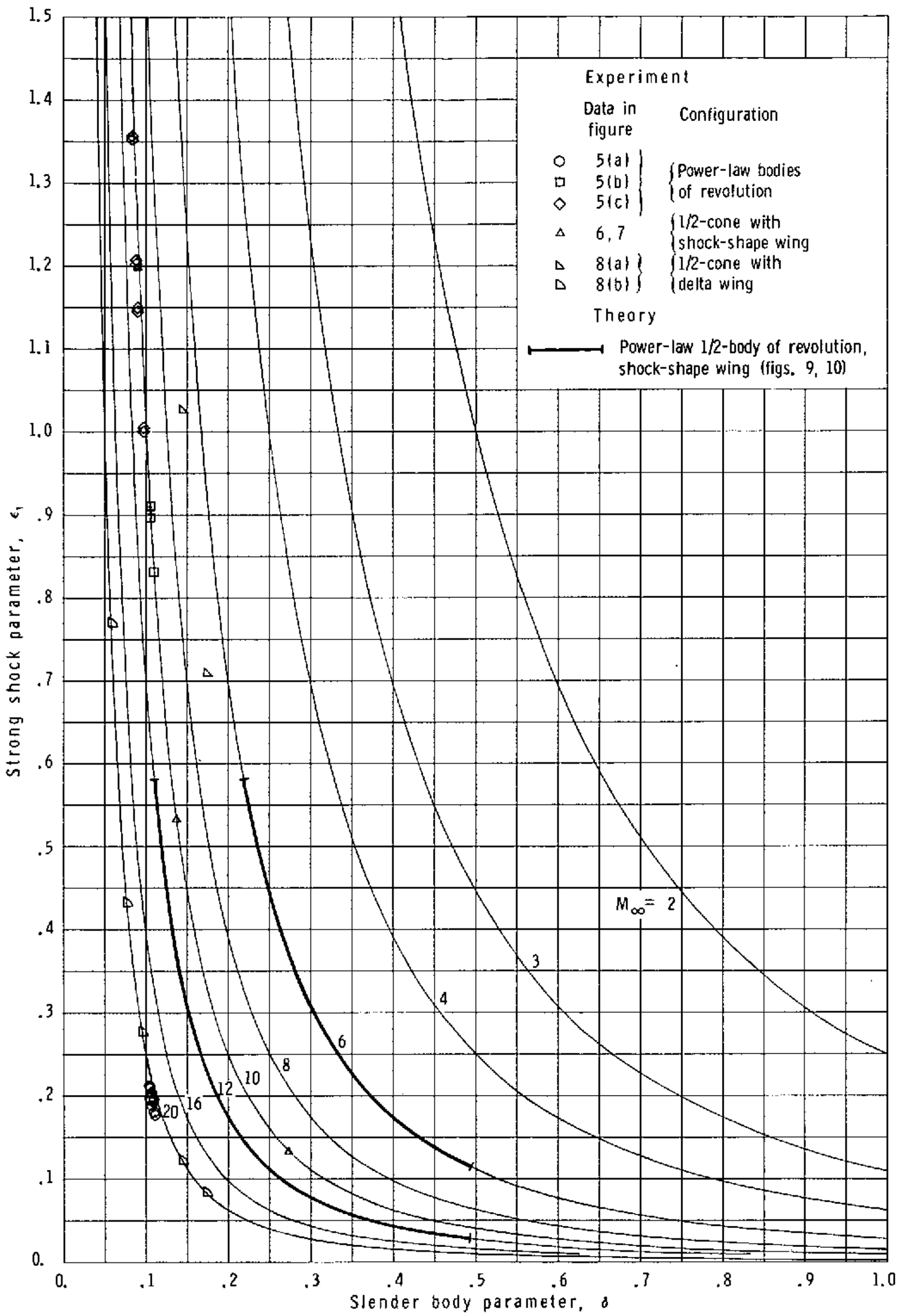

Figure 2.- Graph of the relation $\epsilon_1 = 1/(M_\infty \delta)^2$ for several Mach numbers and showing the values of δ and ϵ_1 for various sets of experimental data.

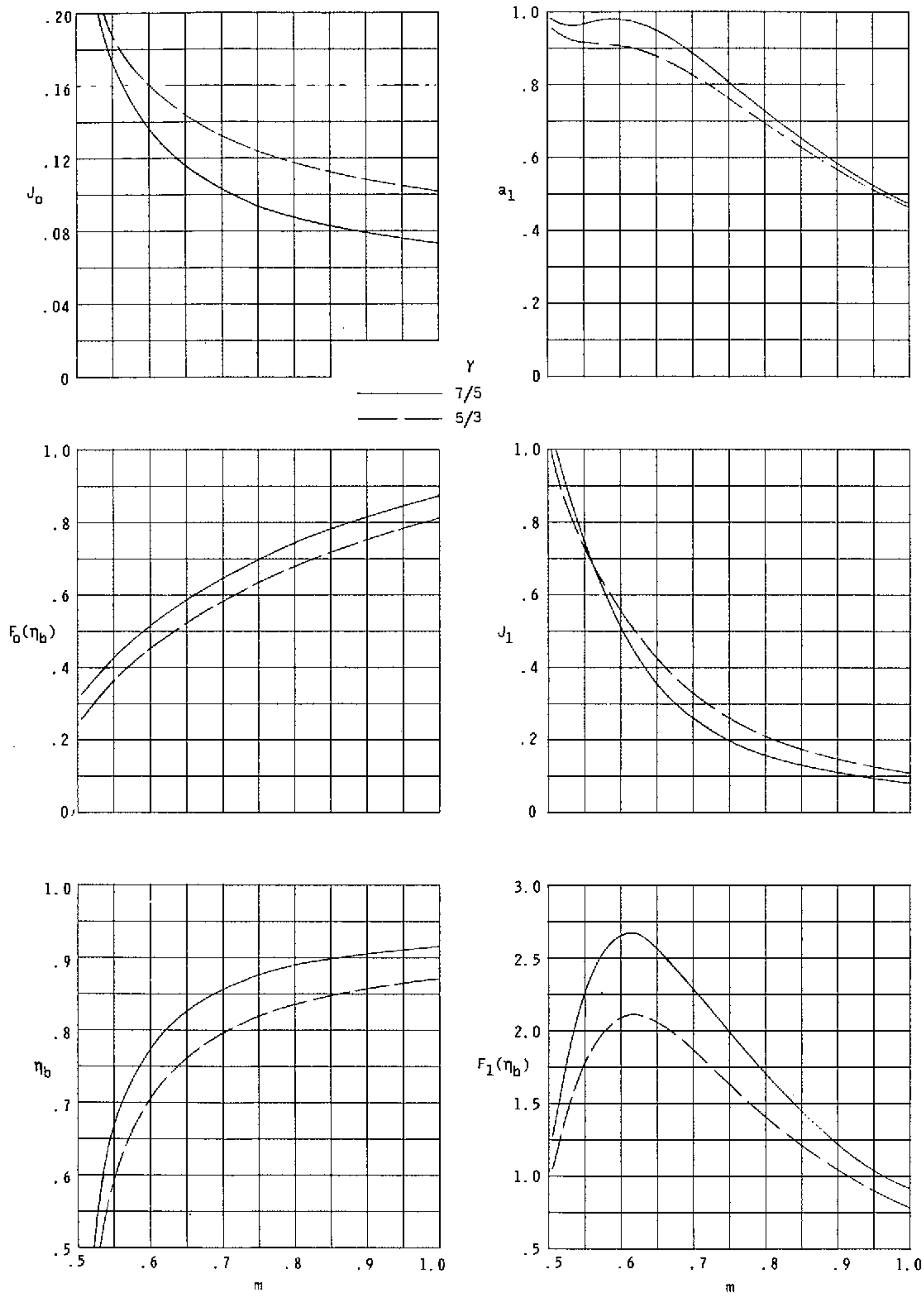

Figure 3.- Variation of similarity solution parameters with power-law exponent m.

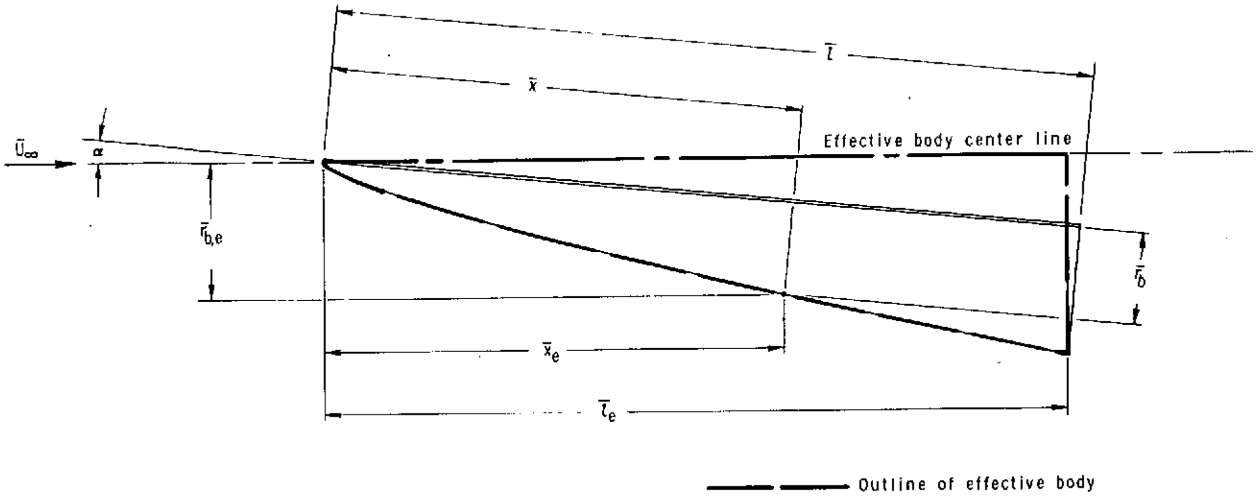

Figure 4.- Effective body for estimating aerodynamic characteristics at angle of attack (shown for $f = 6$, $m = 2/3$).

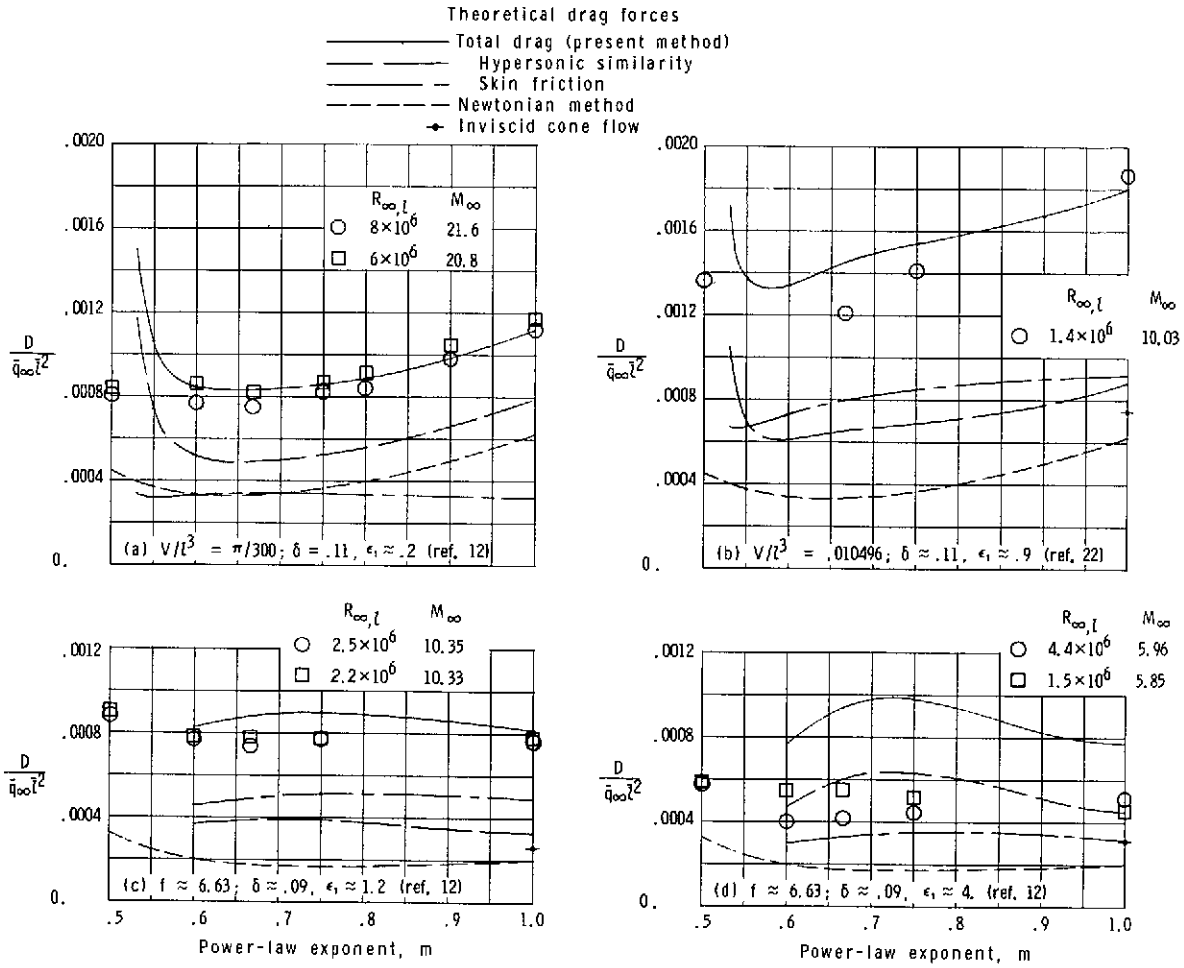

Figure 5.- Comparisons of theoretical drag coefficient at zero angle of attack with experiment for power-law bodies of revolution. The theory is shown for the larger Reynolds number in each case.

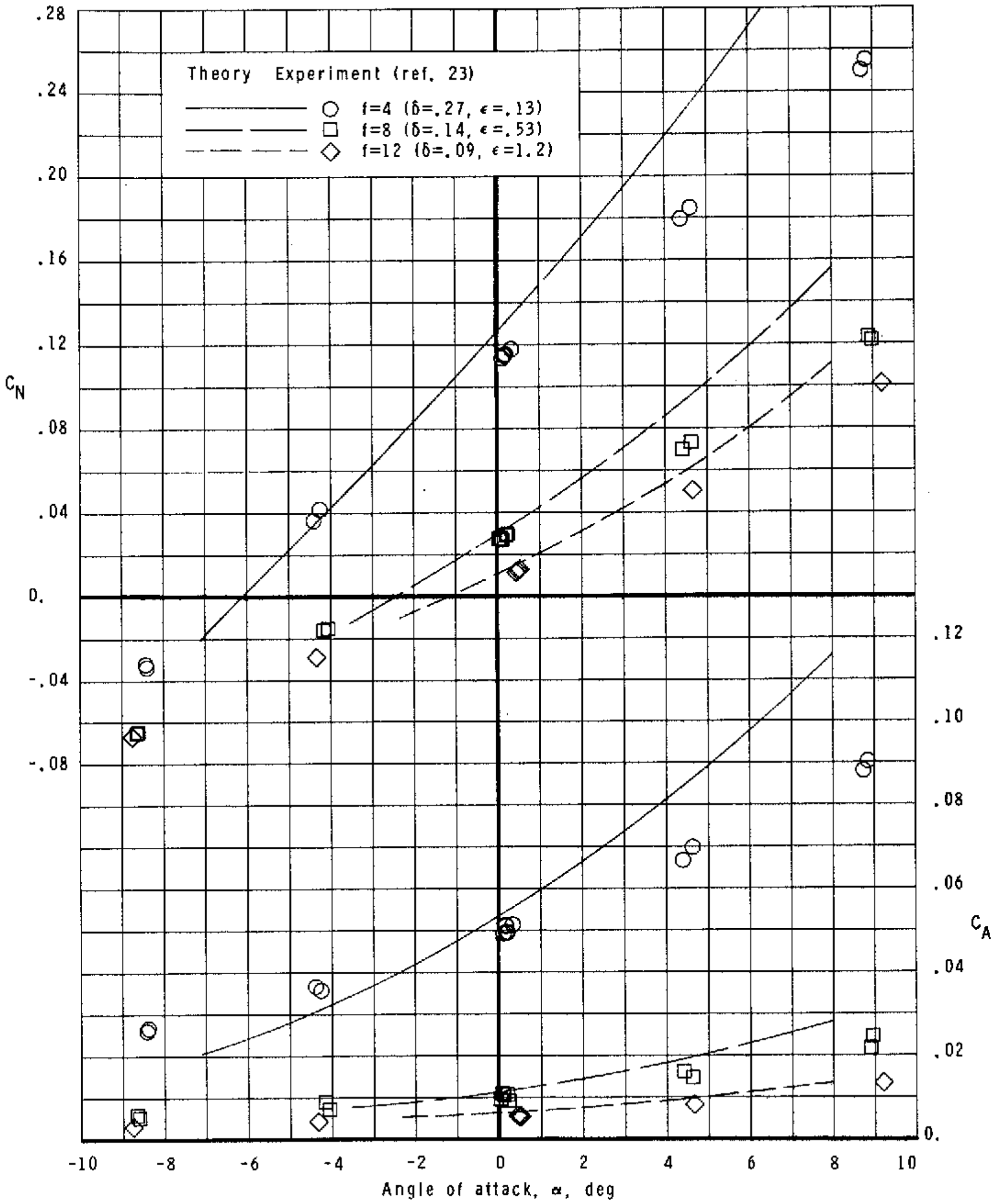

Figure 6.- Comparison of theoretical normal and axial forces with experiment for wing—conical-body configurations (m = 1) at Mach 10.03.

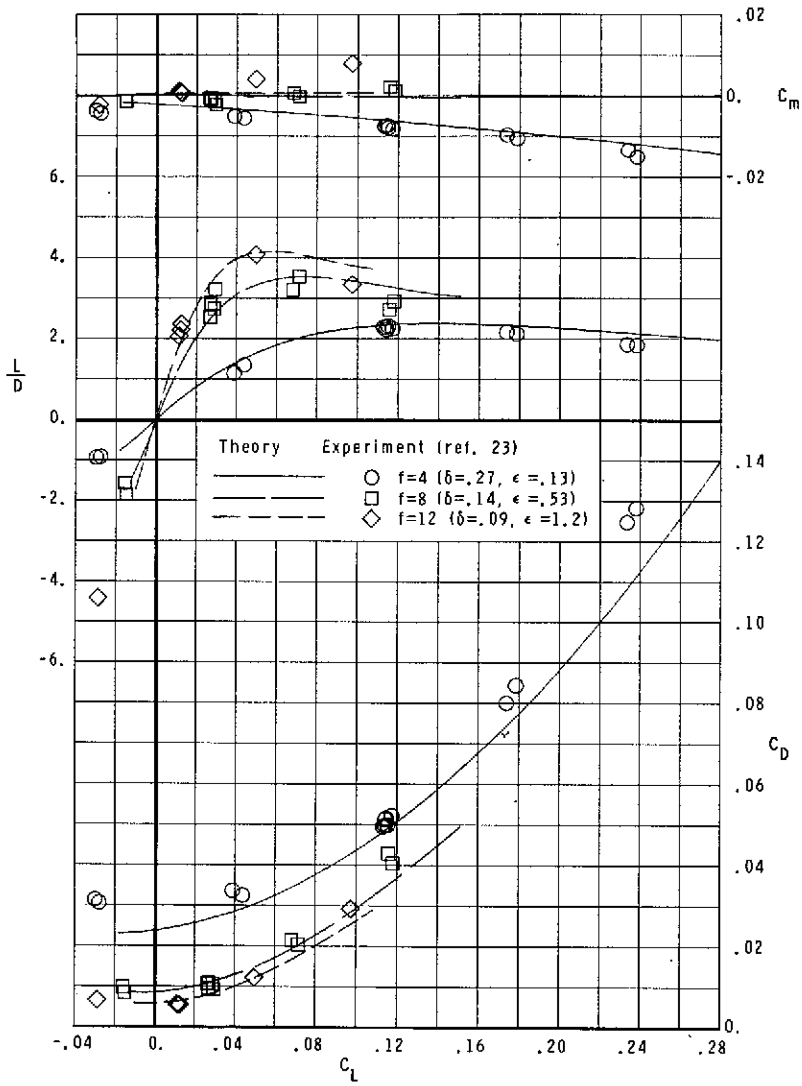

Figure 7.- Comparison of theoretical drag polar, lift-drag ratio, and pitching-moment curves with experiment for wing—conical-body configurations (m = 1) at Mach 10.03.

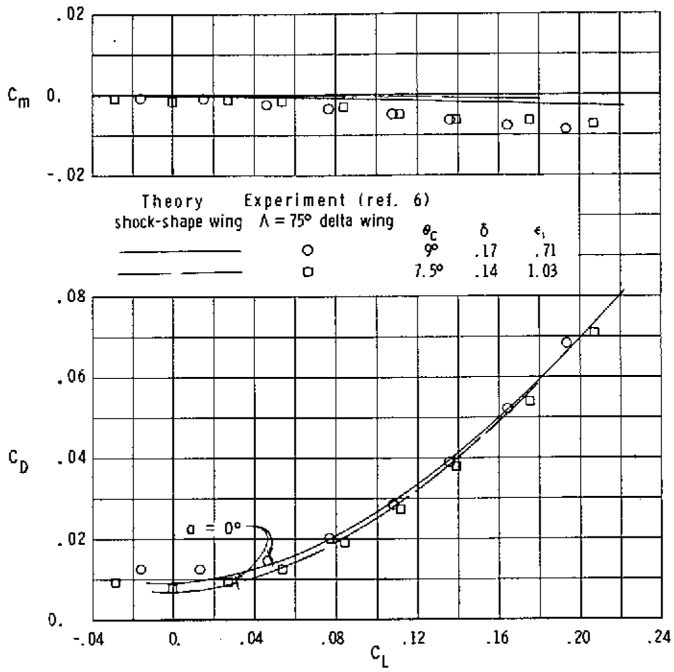

(a) Drag polars and pitching moment at Mach 6.86 in air.

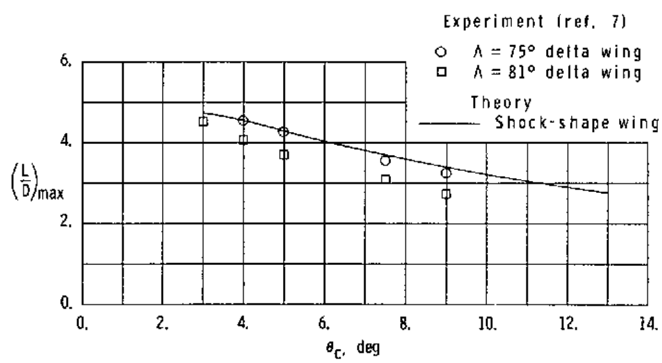

(b) Maximum lift-drag ratio at Mach 19.9 in helium.

Figure 8.- Comparisons of calculated performance of half-cone bodies having shock-shape-matching wings with experimental data for the same bodies having delta-planform wings.

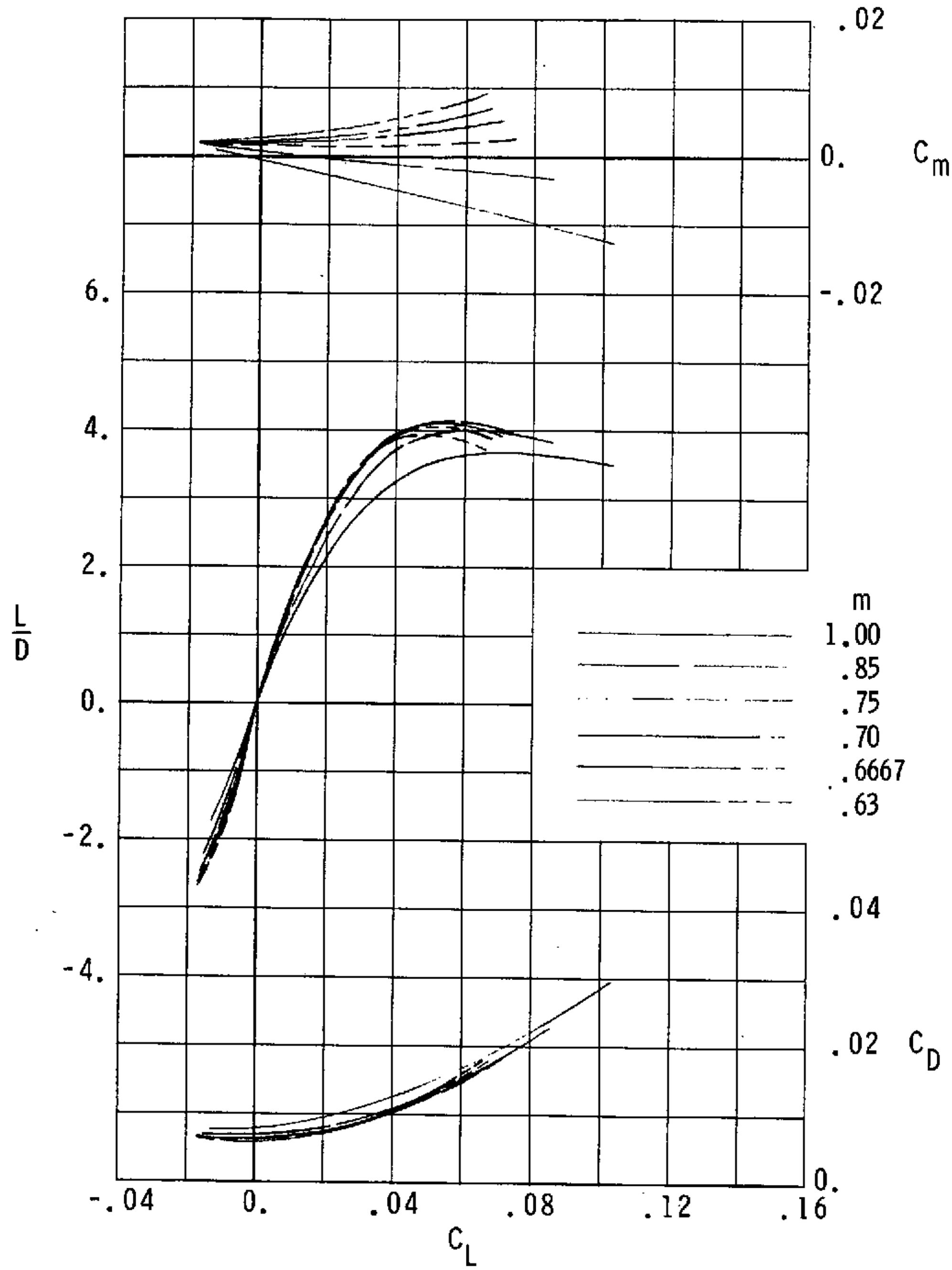

(a) Variation with m for f = 5.

Figure 9.- Comparison of calculated aerodynamic characteristics for Mach 12 flight at an altitude of 30 km. Volume = 2500 m^3; moment reference center at $\bar{x} = 0.6\bar{l}$, $\bar{y} = 0.15\bar{r}_{b,B}$.

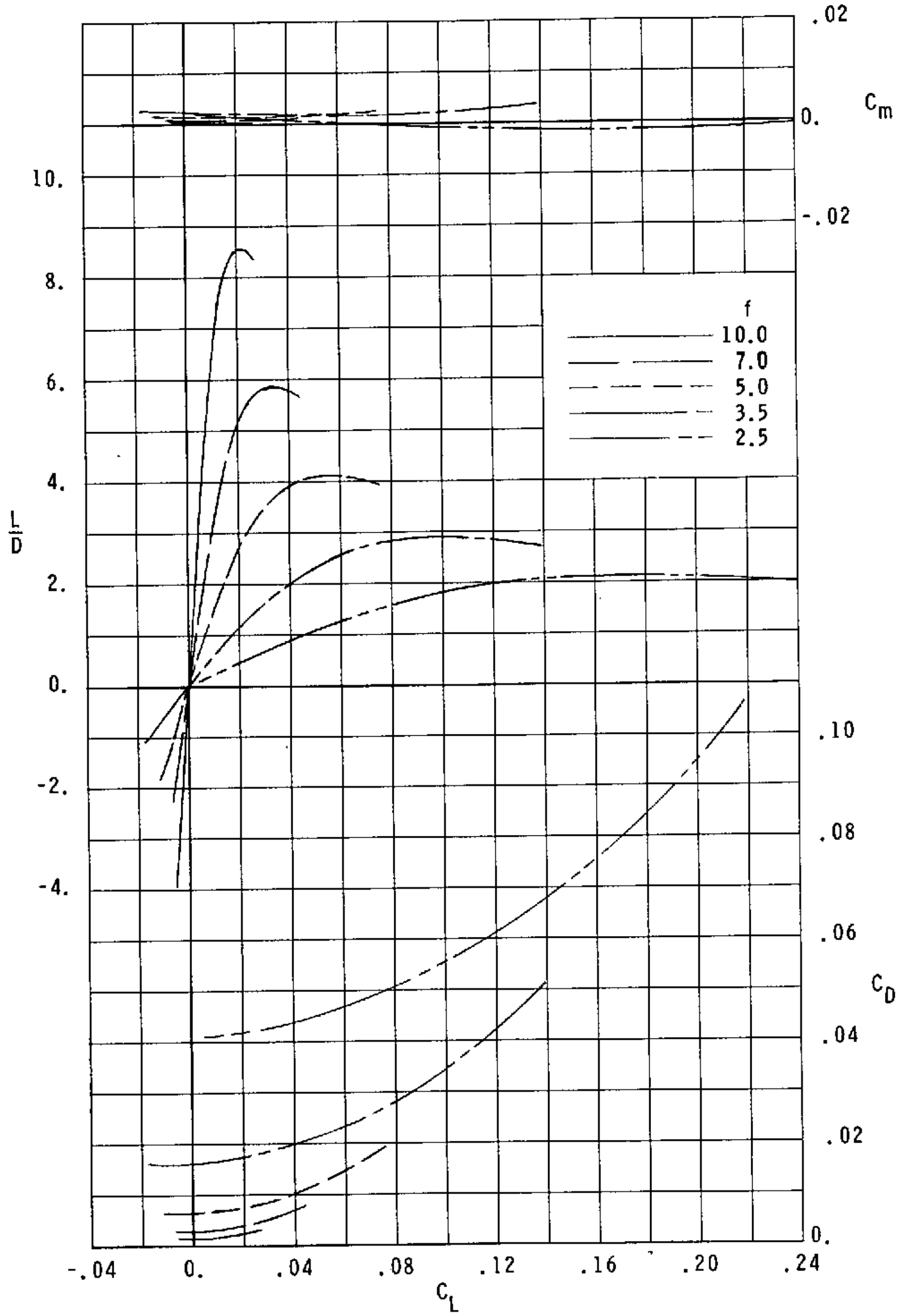

(b) Variation with f for m = 0.75.

Figure 9.- Continued.

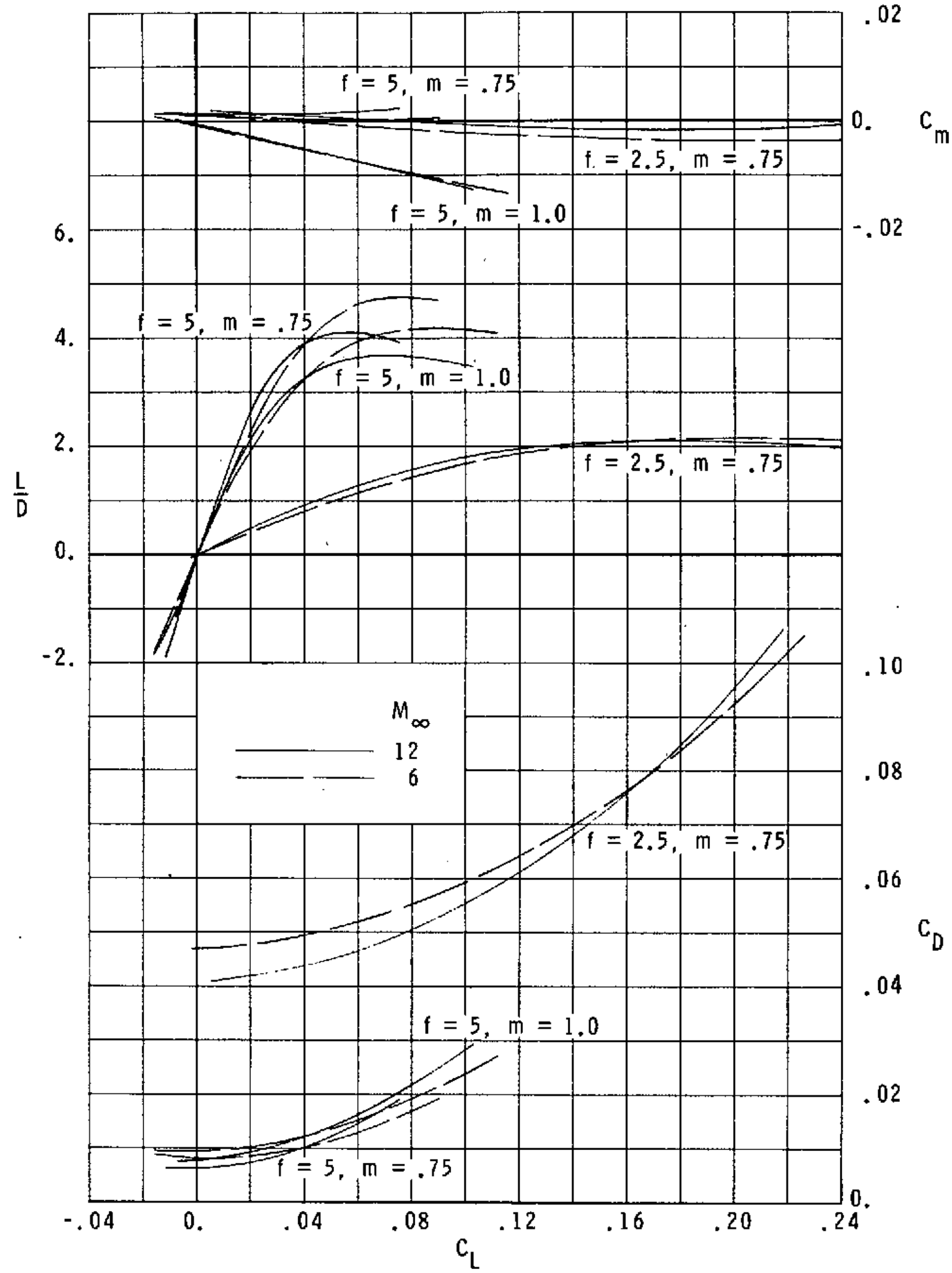

(c) Comparison of three configurations with Mach 6 designs for the same body shapes.

Figure 9.- Concluded.

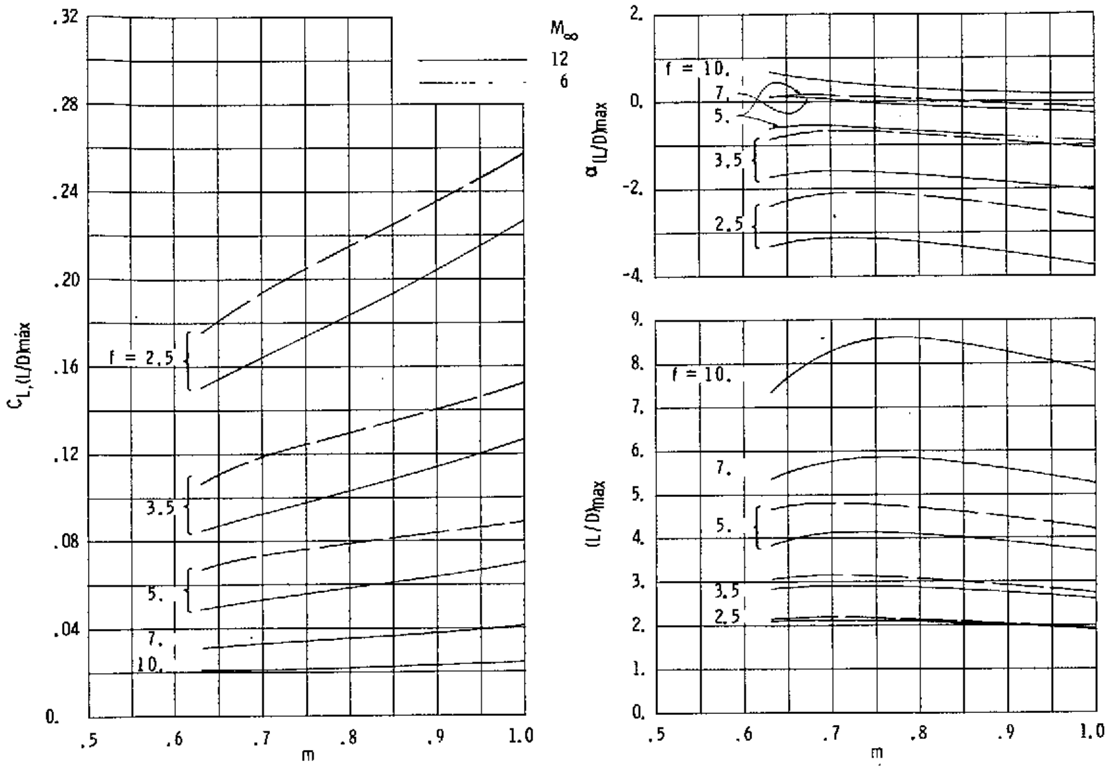

Figure 10.- Summary of theoretical aerodynamic characteristics for configurations of volume 2500 m^3 at Mach 6 and 12 and at an altitude of 30 km.